

FRAGMENTS OF OCEANIC ISLANDS IN THE KURAI AND KATUN' ACCRETIONARY WEDGES OF GORNY ALTAI

N.L. Dobretsov, M.M. Buslov, I.Yu. Safonova, and D.A. Kokh

Institute of Geology, Siberian Branch of the RAS, 3 prosp. Akad. Koptyuga, 630090, Novosibirsk, Russia

The paper presents new data on the structure and composition of the Vendian-Early Cambrian oceanic crust of the Paleo-Asian ocean, which has been fragmentally preserved in Early Cambrian accretionary prisms of Gorny Altai. Mid-oceanic ridge and oceanic island basalts are recognized on the basis of their geochemical characteristics and the composition and geological relationships of volcanogenic and sedimentary units. Our data indicate that hot-spot and mid-ocean ridge volcanism was active in the early stages of the Paleo-Asian oceanic evolution, from Vendian to Early Cambrian.

The study of paleo-oceanic islands incorporated in accretionary-collisional belts is important for the reconstruction of ancient oceans and understanding of endogenic processes that resulted in the formation of the oceanic lithosphere.

Vendian-Cambrian, oceanic crust, Paleo-Asian ocean, MORB, OIB

INTRODUCTION

Fragments of paleo-oceanic lithosphere are preserved in foldbelts, representing large fragments of island arcs and relics of paleo-oceans. In previous studies, various types of ophiolites had been commonly identified as oceanic crust fragments [1–4]. During recent years, numerous fragments of oceanic islands (seamounts) have been distinguished in foldbelts of different ages. It is important that these fragments comprise not only oceanic-type basalts but also larger siliceous-carbonate terranes resembling analogous sedimentary rocks of, for example, fore-arc troughs and marginal seas.

The general problem is that oceanic islands and basaltic plateaus in modern oceans constitute significant volumes and areas in comparison with island arcs (Fig. 1). The elevation of oceanic islands and plateaus above the oceanic floor ranges from 1.5 to 5 km, the thickness of crust varies from 10 to 35 km (as in island arcs), and the area varies from 100 km² for individual islands to 100,000 km² for oceanic plateaus, e.g. Shatsky, Ontong-Java, Kerguelen. Therefore, we can expect that fragments of such structures should be widespread in foldbelts and their volume should be comparable with that of island-arc fragments. The fact that they are less common in folded areas can be explained either by their subduction or by difficulties of their recognition among other sedimentary and basaltic-sedimentary terranes. A possibility for preservation of the fragments of oceanic islands and oceanic plateaus was discussed in [5, 6].

After some simplification, we propose four scenarios for collision of oceanic islands and subduction zones.

1. If oceanic crust thickness is less than 14 km, and the height of oceanic rises is less than 2 km, most oceanic islands and plateaus would be completely subducted and only small fragments can be preserved in olistostromes. This scenario is suitable for all the examples of subduction of oceanic rises providing no significant re-organization of the subduction zone and reported in [7–9].

2. If oceanic crust thickness is 14–20 km, and the height of oceanic rises ranges from 2 to 4 km, larger fragments can be preserved, e.g., sedimentary or basaltic-sedimentary tops of islands. Examples are described by Chekhovich [6].

3. If oceanic crust thickness is 20–30 km, and the height of rises is more than 4 km, oceanic islands could be accreted to an island arc or partly/completely “swallowed” up by a subduction zone. The possibility of such

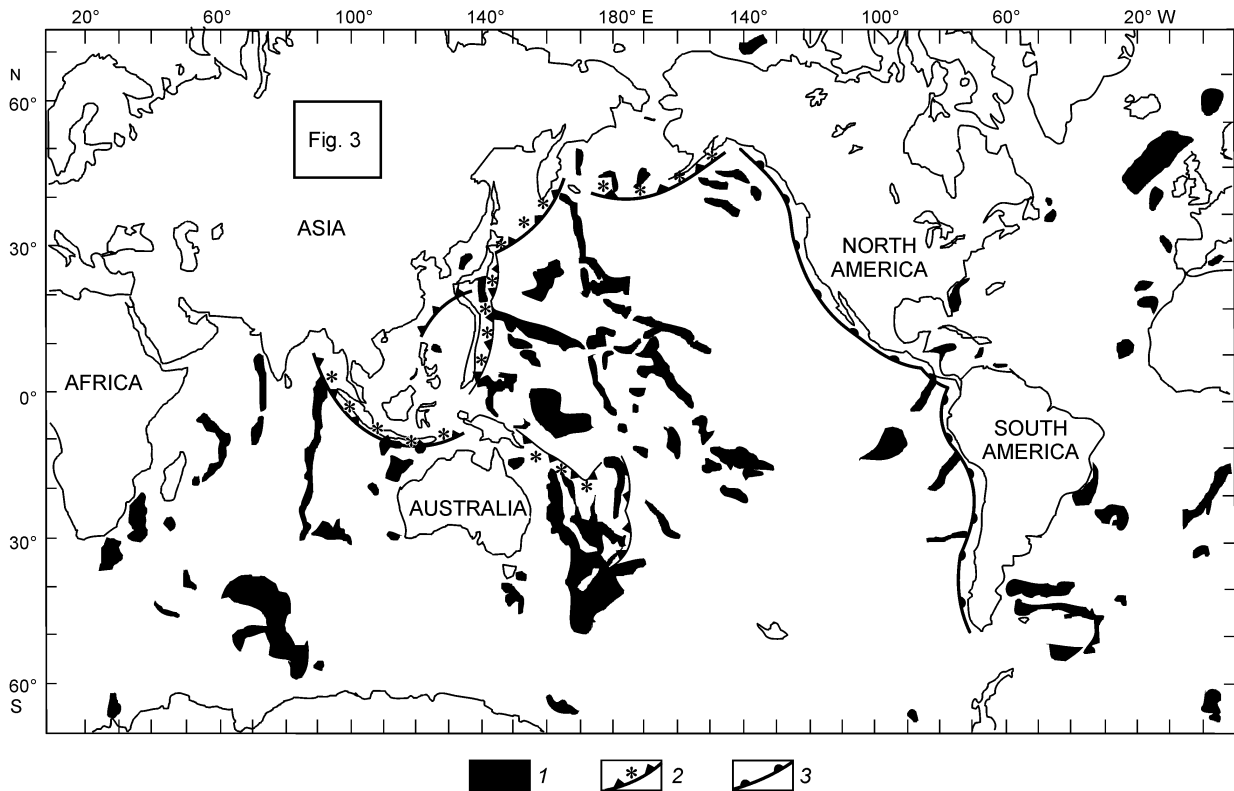


Fig. 1. The distribution of oceanic islands and islands in the world's oceanic basins (modified from [42]).
1 — oceanic islands and plateaus, 2 — island-arc systems, 3 — active continental margins.

transformations and velocity of exhumation depend on the age and velocity of subduction, total weight of an island and rheological properties of rocks [10, 11].

4. If oceanic crust thickness is more than 30 km, the rises higher than 4 km will be incorporated into accretionary wedges as relatively large terranes. Examples are the Akiyoshi terrane in Japan (Kanmera and Sano, 1991), and several terranes in Gorny Altai as described in this paper.

A lasting study of the Akiyoshi terrane [12] showed the presence of shallow-water reef limestones on top of an oceanic island and slope sedimentary facies composed of carbonate-siliceous rocks of spiculites, underlain by deep-water foot-hill radiolarites and turbidite siliceous and carbonate-siliceous silts, sandstones and siliceous tuffs bounding the slopes of the islands (Fig. 2).

Paleogeographic reconstruction of oceanic sedimentary rocks was based on (1) the restricted distribution of terrigenous material, (2) coeval accumulation of carbonate and siliceous units overlying basalts and underlain by siliceous tuffs with radiolaria, and (3) the presence of lateral transition between massive limestone and the radiolarian chert succession through the detrital limestone succession containing spicular chert interbeds and a spicular chert succession containing lenses of redeposited limestone. These rocks were deposited simultaneously and have close lateral relationships.

The paper presents the data obtained by the authors during the past 10 years in the Altai-Sayan area (Gorny Altai) concerning the structural position of oceanic island fragments, their composition, microstructure, age, and diagnostic features including geochemistry of basalts, composition and structure of associated olistostromes.

TECTONIC SETTING

The southern framework of the Siberian continent (Fig. 3) is a Caledonian accretion-collisional structure containing fragments of Vendian-Early Cambrian island arcs formed during the closure of the Paleo-Asian ocean [13–22]. In the Vendian-Early Cambrian, an extended system of island arcs existed between the Paleo-Asian ocean and the Siberian continent. In the present-day structural pattern of southern Siberia and Mongolia, the fragments

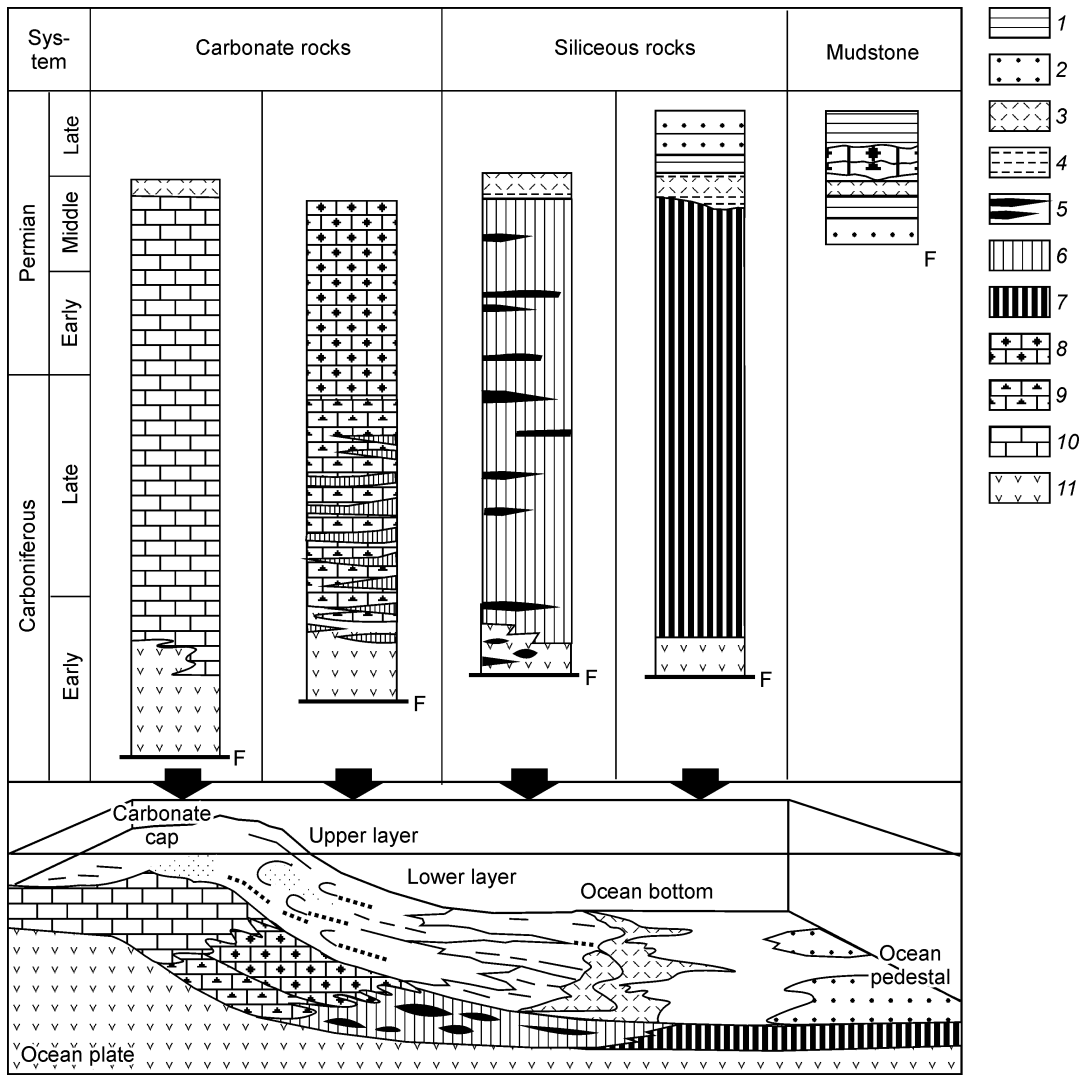


Fig. 2. Composite columnar sections summarizing the lithostratigraphy and age of Akiyoshi terrane rocks and the sedimentary-framework model for oceanic rocks [12]. 1 — mudstone, 2 — sandstone, 3 — silicic tuff, 4 — siliceous mudstone, 5 — displaced mudstone, 6 — spiculite (chert), 7 — radiolarian chert, 8 — limestone conglomerate, 9 — detrital limestone, 10 — reef limestone, 11 — basaltic rocks, F — fault.

of the Vendian-Early Cambrian ophiolites, island arcs and paleo-oceanic islands are incorporated into Early Caledonian accretion-collision units which were separated by Late Paleozoic strike-slip faults.

Temporal and spatial changes in composition of igneous rocks are typical of Altai-Sayan volcanic arcs. Vendian and earliest Early Cambrian tholeiite-boninite series of the early stage reveal similarities to boninites in the Bonin Islands, Mariana and Tonga arcs. Tholeiite-calc-alkaline and, to a lesser degree, calc-alkaline normal arc volcanic series of the later stage, are similar to rocks of the mature Japan, Kuril, and Kamchatka volcanic arcs. Laterally, volcanic units within large fragments of normal island arcs range in composition from tholeiitic high-Mg andesite and basalt rocks near fore-arc basins, through calc-alkaline rocks in the central parts to shoshonitic rocks in back-arc basins [13, 21].

There are three main accretion-collision stages in the evolution of the Paleo-Asian ocean in Gorny Altai and Salair: (1) Early-Middle Cambrian, (2) Late Cambrian-Early Ordovician, and (3) Late Paleozoic [13–16, 22, 23]. The first and second stages characterize the evolution of the Kuznetsk-Altai and Salair island-arc systems. In the Late Cambrian-Early Ordovician, these island-arc systems accreted to the Siberian continent, which led to folding

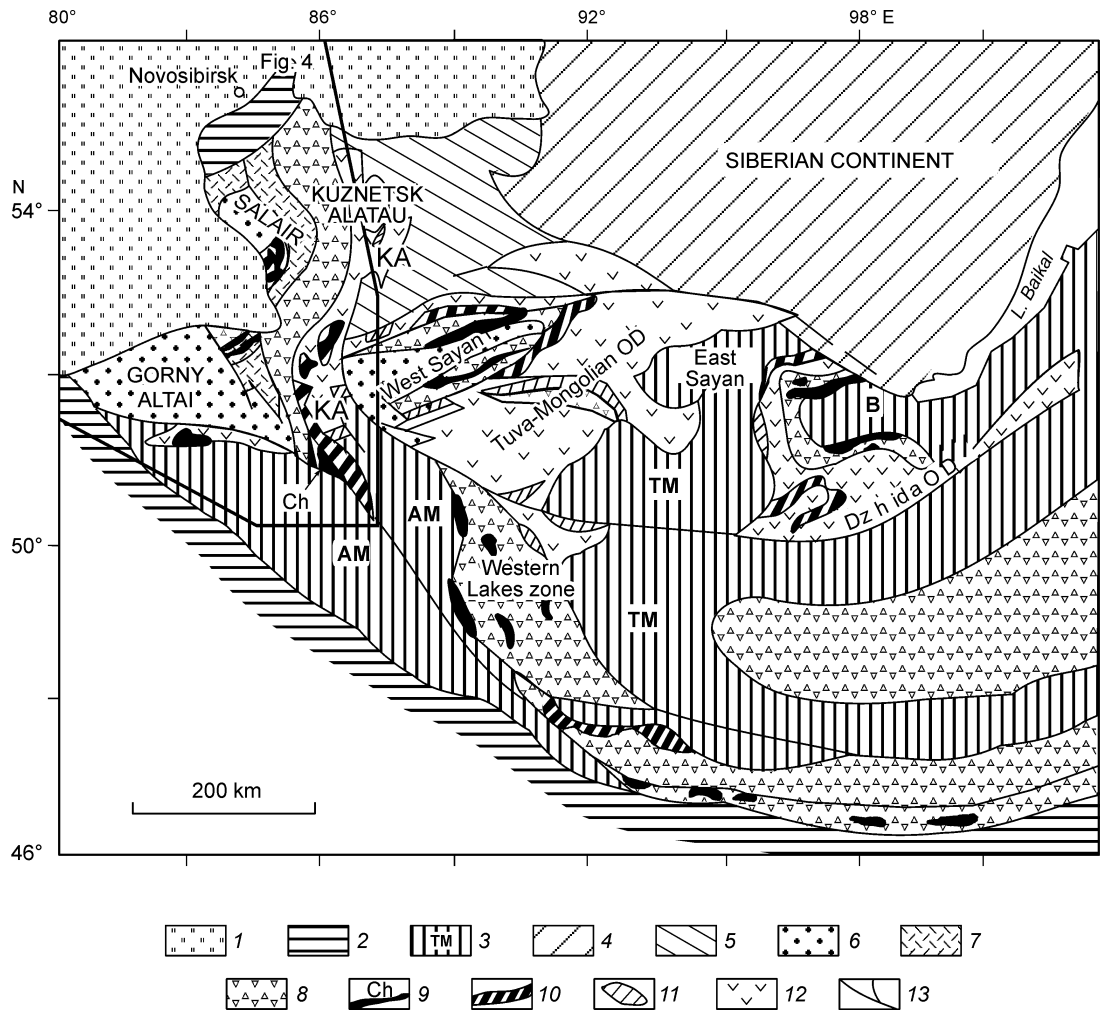


Fig. 3. The Vendian-Cambrian island arc fragments in the framework of the Siberian continent [18]. 1 — Cenozoic depression; 2 — Hercynides of the Ob'-Zaisan and Tom'-Kolyvan' folded area; 3 — microcontinents: Tuva-Mongolian (TM), Barguzin (B), Altai-Mongolian (AM), 4 — Siberian continent; 5–12 — Caledonian folded areas: 5 — Devonian basin, 6 — Cambrian fore-arc trough, 7 — Cambrian calc-alkaline magmatic arcs, 8 — Early Cambrian accretionary prism, 9 — Vendian oceanic ophiolites (ChU — Chagan-Uzun massif), 10 — island arc with boninite-bearing ophiolites, 11 — back-arc basin ophiolites, 12 — island arc; 13 — faults. KA — Vendian-Cambrian Kuznetsk-Alatau island arc.

and thrusting, with a subsequent Early Ordovician hiatus in the stratigraphic records of the studied area. The third stage includes two collisional events during the closure of the Paleo-Asian ocean. The first event corresponds to the collision of the Gondwana-derived Altai-Mongolian terrane with the Siberian continent and the second one was the collision of the Siberian continent together with the Altai-Mongolian terrane with the Kazakhstan continent during the closure of the Paleo-Asian ocean. In the late Paleozoic, the accretion-collision structure of the Siberian continent was disrupted by large-scale strike-slip faults which created a typical mosaic-blocky structure of southern Siberia and Mongolia.

Because of the late Paleozoic large-scale strike-slip faulting, the above-mentioned lateral zoning features of the Vendian-Cambrian island-arc system can be seen only fragmentally in the present-day structural pattern of southern Siberia and Mongolia. They have been better preserved in the western part of the Altai-Sayan folded area, in particular, in Gorny Altai (Fig. 4).

In Gorny Altai, the paleo-oceanic island units (Katun' and Baratal terranes) consist of pillow lavas and related

chert-limestone sedimentary rocks. The Baratal terrane is 70×20 km in size. The Katun' terrane is more than 120 km long and up to 40 km wide. These terranes are incorporated into the Katun' and Kurai accretionary wedges, respectively, alternating with thrust sheets of olistostrome and ophiolites.

The outcrops of the Katun' and Baratal terranes consist of oceanic tholeiites in the base and subalkaline high-Ti basalts, typical of oceanic islands, in the upper part [13, 14, 24–26].

The Kurai accretionary wedge comprises the most complete set of the fragments of paleo-oceanic islands, olistostromes, ophiolites and high-pressure rocks. This allowed a detailed reconstruction of paleogeodynamic processes at the early stages of formation of Gorny Altai structures resembling the modern active margin of the western Pacific [14, 22].

THE STRUCTURE OF THE KURAI ACCRETIONARY WEDGE

The Cambrian accretionary prism (Fig. 5) hosts slivers of the Baratal oceanic island having variable composition and size including oceanic sediments and oceanic island basaltic units alternating with olistostromes, oceanic ophiolites and serpentinitic *mélange* with the slivers and minor blocks of eclogite, garnet amphibolite and barroisite-actinolite schists. The barroisite-actinolite schists often occur within the accretionary prism as large tectonic lenses.

Sedimentary rocks of the Baratal paleo-island demonstrate changes of facies from shallow-water reef limestone, through deeper-water sedimentary-volcanogenic units, to island-slope facies represented by detrital rocks and alteration products of cherts and limestones. The slivers of paleo-island assemblages alternate with olistostrome lenses and fragments of an exotic terrane, consisting of dark-gray to black “hydrosulfide” limestones.

The Kurai accretionary prism consists of three SW-dipping structural units (Fig. 5).

The 15 km wide and 12 km thick **upper structural unit** is composed of tectonic sheets dipping at 70–80° to the SW. The tectonic sheets and lenses consist of paleoseamount siliceous-limestone and carbonate rocks, olistostrome units (including olistoliths), and dark-gray or black limestone. The Baratal seamount is composed of two types of rocks. (1) Light-gray and gray rhythmically layered brecciated limestones. In places, some layers consist of gray cherts, siliceous shales, primary and secondary hyaloclastic rocks. These sediments were deposited close to active volcanoes, possibly at the bottom of their subwater slopes, because they abound in fine fragments of clinopyroxene, orthopyroxene, and hornblende of igneous origin. (2) Poorly bedded reef gray limestones and dolomites once composed tops of oceanic islands.

The dark-gray and black limestones are different from paleoseamount carbonate rocks. They are of massive texture and contain H₂S with thin interbeds and lenses of black siliceous rocks. The black limestones contain [27] the fragments of garnet, tourmaline, sillimanite, staurolite and corundum from metamorphic rocks. The dark-gray and black limestones may represent an exotic block — a passive margin or a cover of a Gondwana-derived microcontinent [28] — which was transported into the subduction zone together with the crust of the Paleo-Asian ocean.

The olistostromes and olistoliths compositionally match the siliceous-carbonate rocks of the paleo-oceanic island or the exotic terrane. They could have been formed during the subduction of the paleo-oceanic island and exotic terrane into a deep-sea trench.

In the base of the upper structural unit there is a 3 km thick package of sheets composed of carbonate and polymictic olistostrome, siliceous rocks and volcanogenic-sedimentary rocks unevenly metamorphosed under greenschist facies conditions.

Large olistoliths up to tens of meters in size are dominant in the polymictic olistostrome as blocky segments with subordinate amount of tectonized matrix. The olistoliths are basalts, volcanoclastics, siliceous rocks and various limestones. The sand-clay calcareous matrix the olistostrome sequence also includes sand-shale horizons containing well-rounded pebbles of marble-like limestone, dolomite, amygdaloidal andesitic basalt and diabase porphyries which could have been transported into the sedimentation basin from an island arc. The sheets of siliceous rocks may reach many hundreds meters in thickness. They are composed of gray and dark-gray massive or rhythmically layered rocks. The thickness of a rhythm can reach 5 cm. Angular-clastic rocks cemented by silica-rich material are found at the base of the rhythmic sequence. The clastic rocks are overlain by fine-grained gritstones and bedded cherts. The presence of clastic material in the polymictic olistostromes suggests its accumulation within a paleo-oceanic trench.

The intermediate structural unit consists of volcanogenic sequence, carbonate sequence, olistostrome, and metamorphic rocks (Figs. 5 and 6).

The basaltic sequence is dominated by pillow lavas and variolitic lavas with geochemical characteristics of

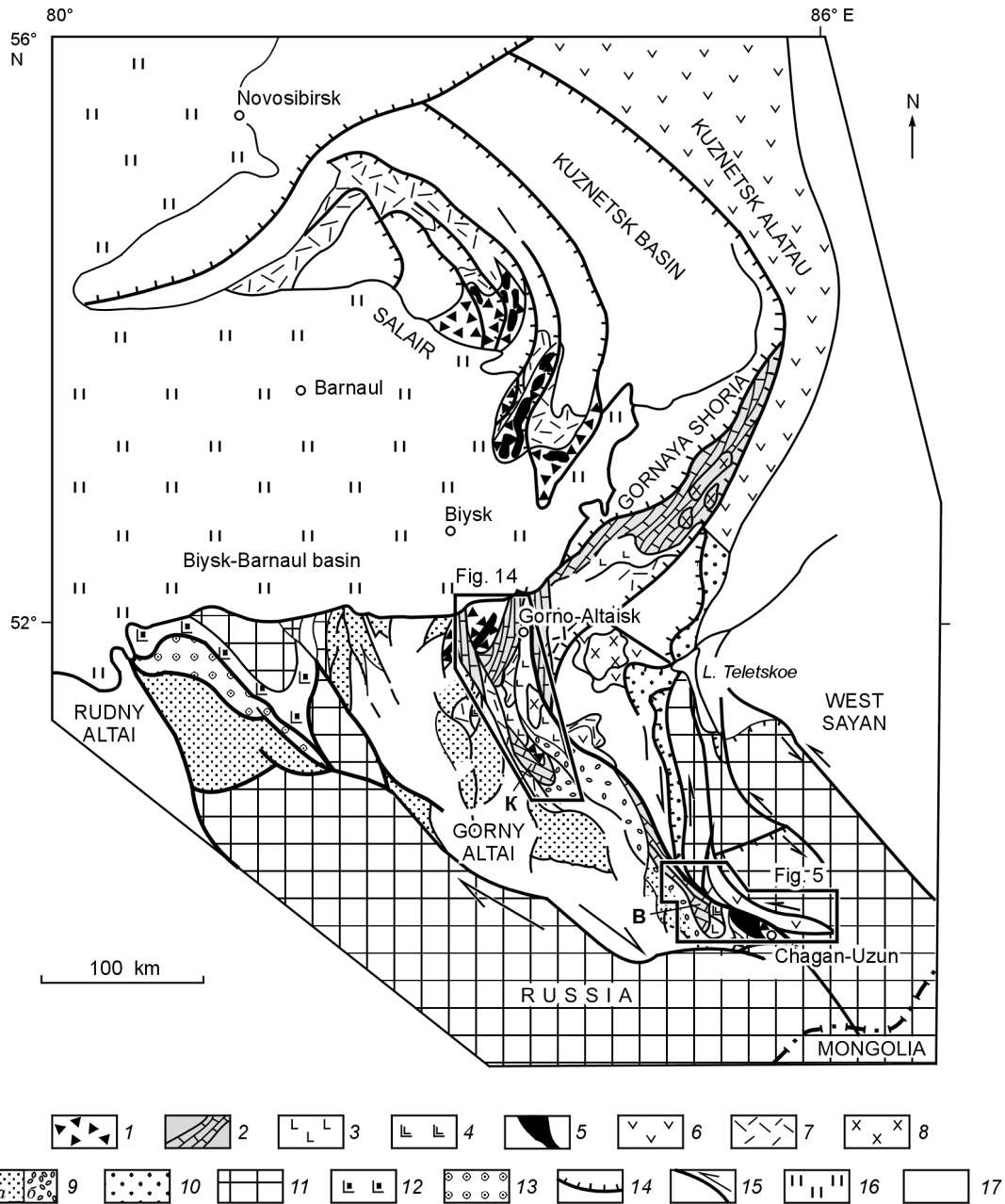


Fig. 4. Vendian-Cambrian island-arc and paleoseamount units in Gornyy Altai. 1–5 — Early Cambrian accretionary wedge: 1 — olistostrome, 2 — oceanic island: K — Katun', B — Baratal, 3 — oceanic island basalts (OIB), 4 — N-MORB, 5 — mafic and ultramafic rocks; 6–10 — Vendian-Cambrian island arc: 6 — tholeiite-boninite series, 7 — calc-alkaline series, 8 — gabbroic massifs, 9 — fore-arc basin (a — flysch, b — olistostrome), 10 — marginal sea sediments; 11 — Precambrian Altai-Mongolian terrane with Ordovician-Devonian cover rocks; 12 — Late Cambrian-Early Ordovician oceanic crust; 13 — Early Ordovician fore-arc trough; 14 — thrust; 15 — strike-slip fault. N-Q — Neogene-Quaternary deposits. Pz₂₋₃ — volcanosedimentary deposits.

OIB and MORB, and also includes minor amounts of amygdaloidal subalkaline basalts, diabase and gabbro-diabase dikes and sills.

The igneous rocks are associated with sparse interlayers and lenses of dark-gray and gray clastic limestone, dolomite, black and gray siliceous rocks and rare volcanomictic sandstone.

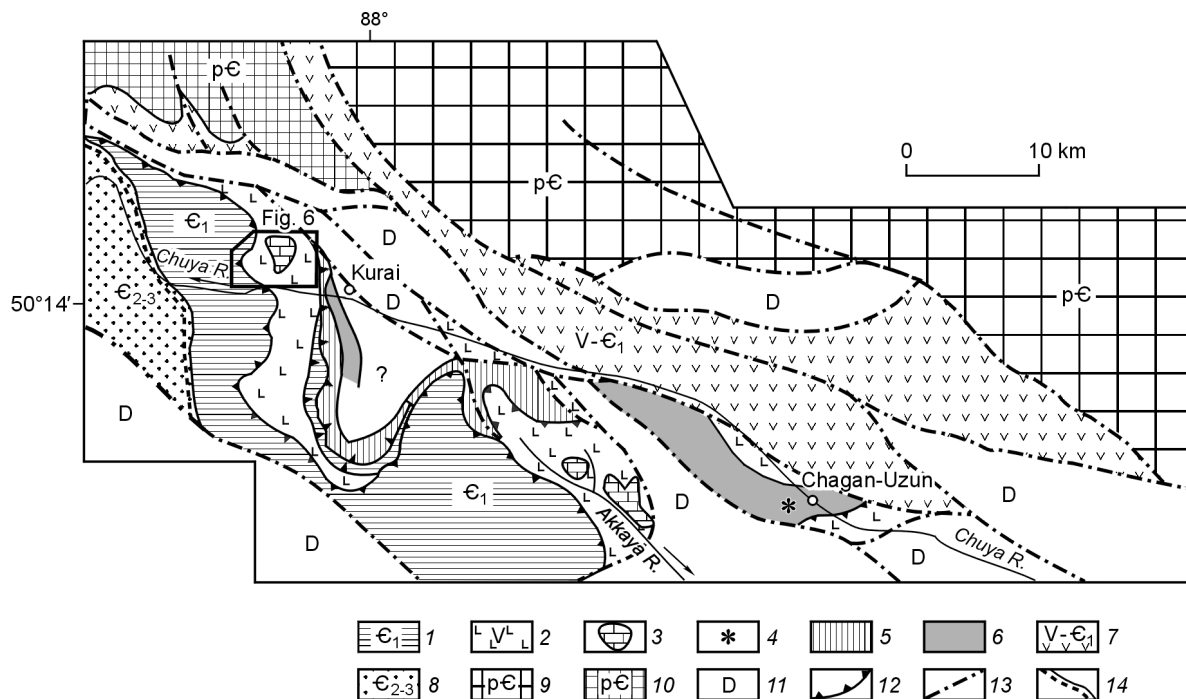


Fig. 5. The geological scheme of the Kurai accretionary wedge. 1 — upper structural unit: Early Cambrian olistostromes, fragments of undivided oceanic units, oceanic plateau and exotic black limestone terranes; 2–3 — intermediate structural units comprising the Baratal paleo-oceanic island: 2 — Vendian oceanic island pillow lavas and volcanogenic sedimentary rocks, 3 — Early Cambrian gray reef limestone and dolomite; 4–6 — lower structural unit: 4 — Early Cambrian eclogites; 5 — Early Cambrian amphibolite and blueschist; 6 — Precambrian-Early Cambrian serpentinite and ophiolites; 7 — Vendian-Early Cambrian Uimen'-Lebed' island arc; 8 — Middle-Late Cambrian Anui-Chuya fore-arc trough; 9 — Precambrian Altai-Mongolian terrane; 10 — Precambrian Teletsk terrane; 11 — Devonian volcanogenic-sedimentary rocks; 12 — Cambrian faults; 13 — Late Paleozoic strike-slip faults; 14 — stratigraphic contact.

The carbonate sequence is mainly composed of dark-gray or reddish reef limestones of layered and massive fabric interbedded with green-gray chlorite-bearing shales and volcanoclastic or, to a lesser degree, graywacke sandstones. The carbonate sequence is the reef “top” of a paleo-oceanic island.

Clastic composition of olistostromes is variable. The olistostromes were formed by collapsing of the frontal part of the Baratal terrane during its subduction. There are two main types of olistostrome. Gritstones and breccias compose the matrix of the first-type olistostrome. There are fragments of gray, light-gray and black cherts and red jasper and smaller amounts of basalt, carbonate, and thin-layered carbonate shales. The gritstones and breccias are cemented by siliceous and carbonate-siliceous rocks and shales and contain olistoliths of mainly siliceous composition with minor basalts and carbonates. The siliceous olistoliths are composed of black and gray silicilith and red jasper. They are of flat or angular shape, up to several tens of meters thick and of hundreds of meters long. Their clastic material could result from disintegration of a silica-rich volcanogenic-sedimentary sequence. Such a sequence could form in a seamount-bottom environment.

The second-type olistostrome has a wider distribution. It consists of sandstone, clay, clay-marl and andesitic tuff matrix and clastics of variable size. Olistoliths comprise siliceous rocks, limestone, dolomite and basalt and can reach hundreds of meters in length and tens of meters in thickness. Most olistoliths are up to 1 m thick and several meters long. Such polymictic olistostromes could have formed in accretionary wedge environment.

Metamorphic rocks occur as large tectonic sheets and are greenschist, amphibolite, and garnet amphibolite.

Volcanogenic, carbonate and sedimentary rocks locally display strong tectonic deformation and compose folded sheets of variable size and internal structure which is discordant with the outer boundaries. The metamorphic

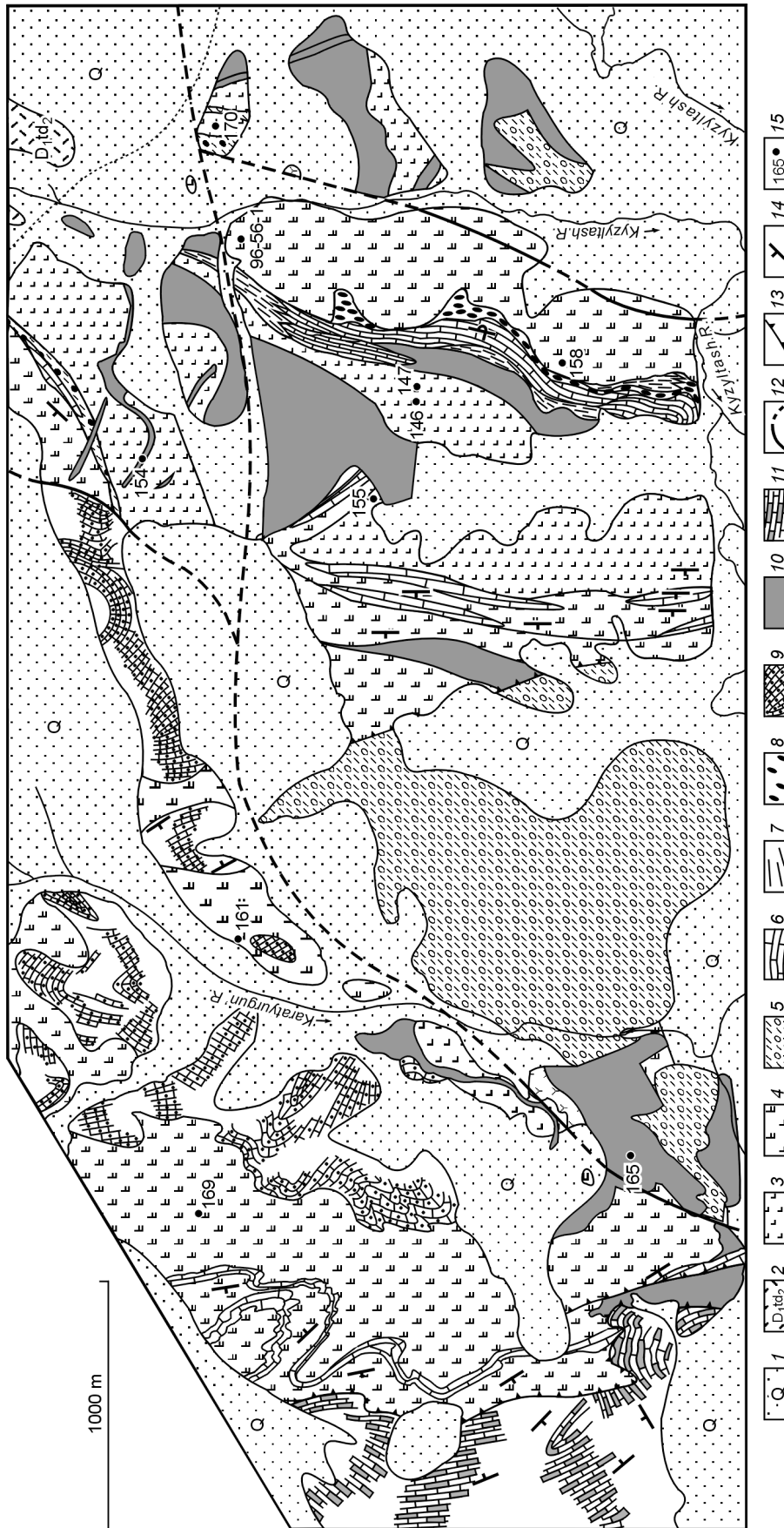


Fig. 6. The detailed geological scheme of the Kurai accretionary wedge northwest of Kurai Village, in the Karatuygun' River basin. 1 — Quaternary; 2 — Early Devonian volcanogenic-sedimentary rocks of the Taldy-Tyurgun' Formation; 3 — Vendian (?) N-MORB-type basalts; 4–10 — Late Vendian units of the Baratal paleo-oceanic island: 4 — volcanogenic sequence with OIB, 5 — slope facies volcanogenic-sedimentary rocks, 6–8 — slope facies volcanogenic-carbonate-siliceous-conglomerate rocks, overlying ophiolites; 6 — carbonate, 7 — chert, 8 — conglomerate; 9 — reef limestone; 10 — dikes of OIB-type basalts; 11 — Precambrian (?) hydrogen sulfur limestone composing an exotic terrane; 12 — Devonian diabase dikes; 13 — strike-slip fault; 14 — thrust; 15 — dips and strikes; 16 — sampling locality.

sequence contains two sheets of crystalline schists (garnet amphibolite and amphibolite) hosted by volcanogenic and sedimentary rocks and dipping westward at 70°, with their thickness ranging from 50 to 250 m in the strike. They show traces of diaphthoresis and melange processes. Locally, they contain blocks of coarse-grained garnet amphibolite hosted by greenschist diaphthorized rocks.

Fresh garnet amphibolite contains zoned garnet with poikilitic quartz, amphibole, and titanite. The amphibolites and garnet amphibolites have chemical characteristics of N-MORB [13, 26].

The 3 km thick **lower structural unit** — the 3 km thick Chagan-Uzun sheeted-melange zone underlying the upper and intermediate units. The sheeted-melange zone (Fig. 5) is located south of Kurai Village, the Chuya left bank, and is composed of polymictic and serpentinitic melanges. The polymictic melange includes up to several meters long blocks of serpentinitized pyroxene-olivine porphyry, diaphthorized garnet amphibolites with relic eclogite, and amphibolites and matrix consisting of serpentinite schists and mylonites after metamorphic rocks and basalts.

The serpentinitic melange consists of foliated serpentinite incorporating blocks of massive serpentinite and light-gray cryptocrystalline rodingite. The serpentinite bodies up to several meters long extend in the NS direction (Fig. 5).

Near Chagan-Uzun Village, the Chuya left bank, the sheeted-melange zone consists of:

(1) a 3 km thick sequence of tectonic sheets of the Chagan-Uzun peridotite massif. The upper sheet is made up of ultrabasics with serpentinitic mélange in its lower horizon. The sheets of serpentinitic melange up to 100 m thick contain inclusions of massive serpentinites, eclogite-garnet amphibolites and minor greenschists. The largest bodies are composed of garnet amphibolites containing eclogite relics [14, 29]. The K-Ar ages of amphiboles from the eclogite of the upper tectonic sheet and from the zones cutting the garnet amphibolite are 535 and 487 Ma, respectively. The K-Ar amphibole age of garnet amphibolite composing separate sheets is 473 Ma. The Ar-Ar amphibole ages of eclogites from another tectonic sheet are 562 ± 11 , 625 ± 5 and 635 ± 10 Ma [16].

(2) The lower tectonic sheet is composed of massive and schistose serpentinites which contain boudins and deformed dikes of gabbro and gabbro-diabase. The outside zones of these bodies are made up of rodingites. To the east, in the Chuya right bank, all these rocks are melanged and overlain by the upper sheet mélange. The sheets comprise an overturned ophiolitic section with a reduced gabbro zone replaced by mélange.

The upper sheet includes eclogite and garnet amphibolite, which formed at up to 20 kbar and 660 °C, i.e. at a depth of 80 km [30], whereas metagabbro, rodingites and garnet-free amphibolites of the lower sheet — at 2–3 kbar (6–8 km depth) [29].

COMPOSITION OF BASALTS OF THE KURAI ACCRETIONARY WEDGE

Chemical composition of the Kurai metabasaltic rocks is presented in Table 1, which shows bulk-rock chemical compositions of metabasalts sampled at a site near Kurai Village, where primary relationships between paleo-oceanic island units are mapped: between carbonate top and volcanic island and between slope facies at the base and oceanic crust basalts (Fig. 6). The metabasalts in this unit are dominated by fine- to medium-grained amygdaloidal basalt and andesitic basalt with porphyritic texture. The amygdules are filled with calcite and chlorite, and the phenocrysts are plagioclase and clinopyroxene. Groundmass is variolitic or hyalopilitic. These chemically uniform samples have been metamorphosed to the greenschist facies. In the TAS diagram the Kurai metabasalts plot in the field of basalt and trachybasalt (Fig. 7, A), although this classification is not reliable because of the high mobility of potassium and sodium during sea-floor hydrothermal alteration and metamorphism conditions. All are subalkaline basalts, as shown by their low Nb/Y ratios (Fig. 7, B). As FeO* wt% tends to increase with FeO*/MgO, a tholeiitic trend can be supposed (Fig. 8, A). The increase in TiO₂ with FeO*/MgO is not so obvious, suggesting a character intermediate between abyssal tholeiite and island-arc tholeiite (IAT) (Fig. 8, B). Contents of TiO₂ and P₂O₅ range from 0.43 wt.% to 2.3 wt.% and from 0.1 wt.% to 0.58 wt.%, respectively (Table 1); P₂O₅/TiO₂ ratio is >0.15 for samples 158, 161, 165, 169 and 96-56-1 and <0.15 for samples 141–155 and 170; Al₂O₃ ranges from 13 wt.% to 18 wt.%. In general, compared to IAT, the Kurai metabasalts are depleted in LILE (K, Rb, Ba) and have similar or slightly greater HFSE (Zr, Nb, Th, Hf) contents. Three groups of samples may be recognized according to their HFSE and LILE concentrations and Zr/Nb ratios. **The first group** possesses chemical characteristics of N-MORB. This includes samples 146, 154, 155 which are enriched in HFSE and have high Zr/Nb ratios. **The second group** has an affinity to alkaline basalts of oceanic islands and plateaus and includes LILE-high and HFSE-depleted samples 169, 96-56-1, 141, 147, 158, 161 with a low Zr/Nb ratio. **The third group** includes chemically intermediate samples 165 and 170, which we interpret as T-MORB (Table 1) [31, 32]. In the Nb-Zr/4-Y diagram (Fig. 9) sample 169 plots between the N-MORB and OIB fields. The other samples plot in the field of N-MORB.

Table 1
Major and Rare Elements of Basalts from Accretionary Wedges

Component	Kurai												Katun'				N-MORB	OIB
	141	146	147	154	155	158	161	165	169	170	96-56-1	92-S-1	92-S-3	96-38-3	96-48-1			
SiO ₂ , wt. %	49.59	47.25	49.18	46.27	52.36	47.61	47.53	47.29	48.89	48.51	50.15	52.32	47.62	42.26	46.94	49.13	46.46	
TiO ₂	1.23	1.84	1.75	2.36	1.84	1.54	1.78	1.65	0.43	1.45	1.511	2.26	2.4	1.51	3.07	1.17	3.01	
Al ₂ O ₃	14.14	13.67	13.10	12.90	14.17	14.67	16.15	14.60	17.86	13.44	14.57	12.44	13.04	14.79	13.79	15.64	14.64	
Fe ₂ O ₃	14.34	12.91	12.85	14.96	11.24	12.30	12.33	13.57	8.82	13.48	13.76	11.11	13.85	9.40	12.17	9.97	9.85	
MnO	0.44	0.23	0.24	0.25	0.17	0.27	0.21	0.21	0.18	0.24	0.26	0.1	0.14	0.23	0.16	0.16	0.14	
MgO	6.01	7.26	6.94	6.96	4.59	6.59	7.25	6.69	6.23	5.92	3.89	6.19	7.42	6.94	5.26	8.22	8.19	
CaO	4.91	10.00	8.67	6.82	6.32	4.80	5.24	6.95	8.06	6.37	5.44	7.6	8.81	13.59	9.86	11.84	10.33	
Na ₂ O	2.92	3.32	4.23	5.18	4.76	5.32	4.44	4.28	4.75	6.21	5.76	5.04	3.7	3.95	2.36	2.40	2.92	
K ₂ O	1.50	0.29	0.36	0.49	0.70	0.54	0.44	0.44	0.90	0.21	0.71	0.68	0.41	0.46	1.55	0.20	0.84	
P ₂ O ₅	0.13	0.18	0.18	0.23	0.21	0.45	0.43	0.37	0.40	0.10	0.58	0.29	0.31	0.17	0.28	0.12	0.37	
LOI	5.41	2.74	2.37	3.35	2.53	5.42	3.71	3.59	3.13	3.07	3.86	2.76	3.42	6.98	4.76	1.09	—	
Total	100.63	99.68	99.87	99.78	98.89	99.51	99.51	99.63	99.65	99.90	100.54	99.78	99.86	100.27	100.22	—	—	
La, ppm	4.6	5.7	2.8	6.5	5.9	7.5	8	7.2	20	3.2	11	9.5	11	11	17	2.50	37	
Ce	12	16.5	7.4	15.5	18.6	18.6	20.6	16.6	42	8.5	25	24.5	36	25	32	7.50	80	
Nd	7.7	13.2	5.3	12.3	13.7	12.8	15.6	11.4	19.9	6.8	16	15	24.5	16	18	7.30	38.5	
Sm	2.75	4.4	2.1	4.7	4.6	4.3	4.2	3.6	4.1	2.65	5.2	47	5	3.8	5	2.63	10	
Eu	1.1	1.7	0.83	1.65	1.75	1.8	1.88	1.77	1.3	1	2	1.4	1.72	1.2	2	1.02	3	
Tb	0.62	1.09	0.5	0.94	1.11	0.74	0.8	0.74	0.41	0.57	1.1	—	5.2	—	4	0.67	1.05	
Yb	3.2	5	2.15	3.4	4.7	2.7	2.9	2.8	1.4	2.7	3.8	0.82	1.05	0.7	0.8	3.05	2.16	

Table 1 (continued)

Component	Kurai											Katun'				N-MORB	OIB
	141	146	147	154	155	158	161	165	169	170	96-56-1	92-S-1	92-S-3	96-38-3	96-48-1		
Lu	0.56	0.8	0.35	0.6	0.77	0.4	0.43	0.41	0.22	0.48	0.55	1.9	2.2	2.1	2.1	0.46	0.3
Sc	32	41	45	38.6	31.3	24	29.3	27	24	38	19	0.29	0.31	0.3	0.26	40	—
Th	0.38	0.25	0.45	0.35	0.25	0.45	0.5	0.4	0.85	0.18	0.9	23.6	23	39	30	0.12	4
U	0.47	0.2	0.3	0.05	0.04	0.2	0.28	0.13	0.04	0.04	—	0.6	0.6	0.9	1.5	0.05	1.02
Hf	2.1	3.6	1.4	2.9	3.9	1.9	2.1	1.6	0.8	1.6	2	—	—	2.1	4	2.05	7.8
Ta	0.12	0.22	0.1	0.23	0.2	0.21	0.21	0.16	0.1	0.04	0.25	1.1	1.2	0.9	1.4	0.13	2.7
Ba	280	10	50	70	100	260	600	70	300	10	480	—	—	95	350	6.30	350
Co	39	53	47	52	38	38	39	40	24	51	42	—	—	40	56	—	—
Cr	10	100	251	40	25	75	8.5	7.5	10	9.5	—	—	—	100	100	250	—
Rb	34.2	3.1	5	5.46	6.84	6.27	6.45	5.8	17.5	2.79	15	6.5	2.56	5	25	0.56	31
Sr	289	211	255	148	171	327	475	514	852	201	560	120.4	267.8	300	800	90.00	660
Y	35.7	58	28	48.8	61	35.2	38.2	32.6	15.45	35.5	40	23.9	18.7	13	27	28.00	29
Zr	75	157	62	137	186	78	99	72	38.5	73	108	140.8	124.4	80	170	74.00	280
Nb	1.71	4.04	2.25	5.05	4.53	3.68	4.3	3.06	4	1.01	4.00	20.5	17.7	14	26	2.33	48
P ₂ O ₅ /TiO ₂	0.11	0.10	0.10	0.10	0.11	0.29	0.24	0.22	0.93	0.07	0.39	0.13	0.13	0.11	0.09	0.1	0.12
Zr/Nb	43.86	38.86	27.56	27.13	41.06	21.20	23.02	23.53	9.63	72.28	27.00	6.87	7.03	5.71	6.54	4.15	35.20
(Nb/La) _N	0.35	0.67	0.76	0.73	0.72	0.46	0.51	0.40	0.19	0.30	0.34	1.19	1.41	0.70	0.85	0.78	—
(La/Ta) _N	2.33	1.58	1.70	1.72	1.79	2.17	2.32	2.74	12.16	4.86	2.67	0.97	0.65	0.87	0.86	1.14	—
(La/Yb) _N	0.91	0.72	0.83	1.21	0.80	1.76	1.75	1.63	9.08	0.75	1.84	3.37	3.37	3.53	5.46	0.54	—

Note. Major elements are: for N-MORB after average tholeiite MORB [31], for OIB — after subalkali olivine basalts [31]. Rare elements for N-MORB and OIB — after [35].

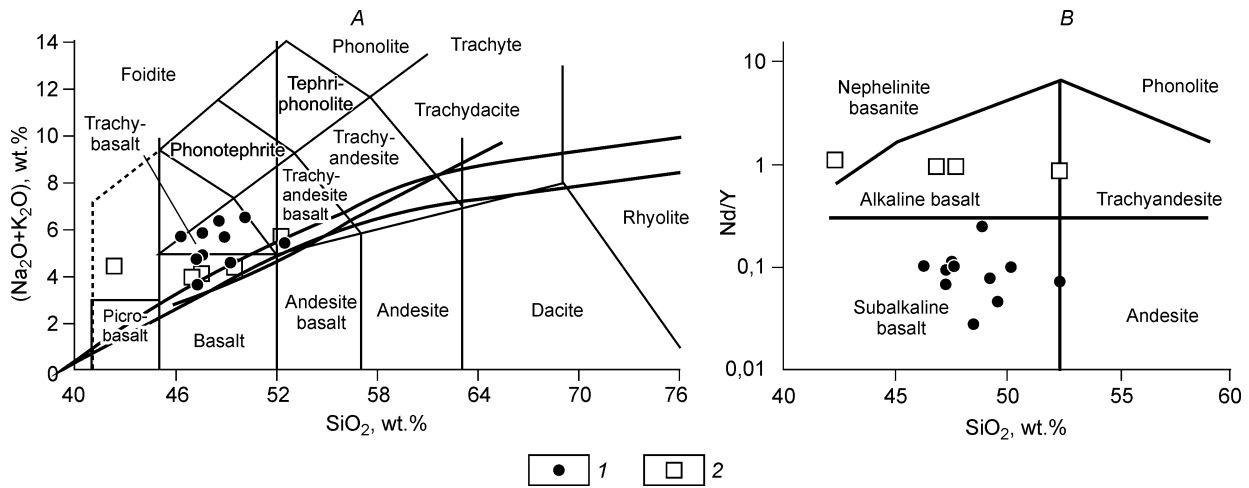


Fig. 7. Petrochemical classification diagrams: A — TAS; B — Nb/Y versus SiO₂ [32]. Metabasalts: 1 — Kurai, 2 — Katun'.

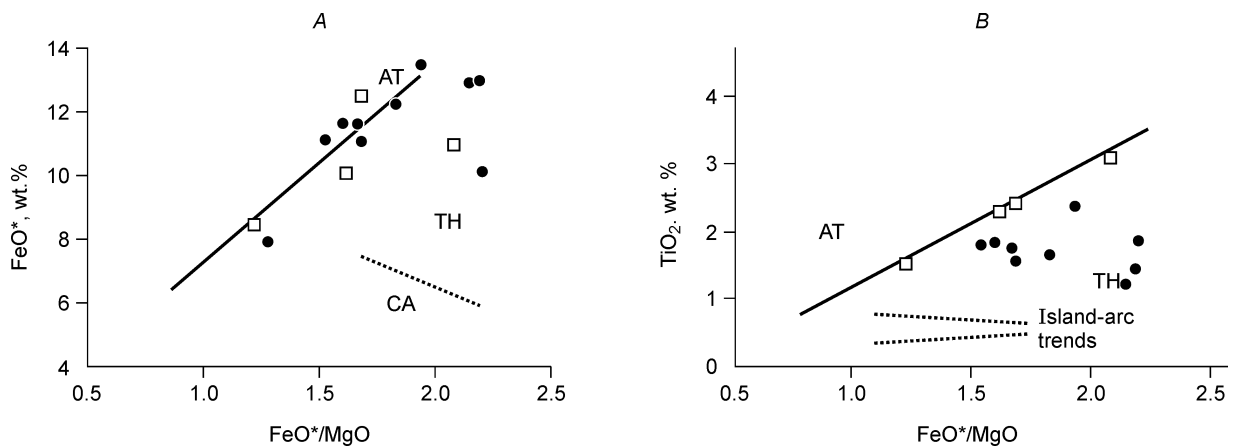


Fig. 8. Major element plots: A — FeO* vs FeO*/MgO; B — TiO₂* vs FeO*/MgO. Discriminant fields and trends of abyssal tholeiite (AT), tholeiite (TH) and calc-alkaline volcanic rocks (CA) are after Miyashiro [38]. Symbols as in Fig. 7.

All but two (nos. 169 and 96-56-1) basaltic samples have very uniform REE patterns (Fig. 10), showing no obvious LREE enrichments, as typical of hot spot basalts, with $La_N = 9-25$, $(La/Yb)_N = 0.151.9$. Samples 158, 161 and 165 show small positive Eu anomalies. This could result from accumulation of plagioclase, which was floating in intermediate magmatic chambers located at the base of the oceanic crust, at a depth greater than 20 km, i.e. under 6–8 kbar. Sample 169, the most differentiated basalt, has the highest LREE abundances but the lowest HREE relative to the basalts, with $La_N = 60$, $(La/Yb)_N = 9.1$ and no Eu-anomaly. Sample 96-56-1 has elevated LREE and intermediate HREE with $La_N = 33$, $(La/Yb)_N = 1.9$ and a small positive Eu-anomaly.

MORB-normalized trace element patterns show lower HFSE abundances and Nb content is almost equal to MORB (Fig. 11). These patterns also resemble those of oceanic plateau basalts (OPB) in the Nauru basin [33]. The Kurai basalts are enriched in incompatible elements relative to MORB, showing the signature of oceanic island basalt (OIB) [34]. Most samples have similar patterns and represent so-called transitional MORB (T-MORB) [32]. The samples are depleted in Cr. This may be explained by fractionation of Cr-spinel from the melt.

In the chondrite-normalized spidergrams (Fig. 12) all basaltic samples have “humped” patterns, probably due to LILE added during secondary alteration, and are characterized by variable enrichment in all the trace elements with respect to chondrite [35]. These samples display mild depletion in Nb-Ta relative to La (i.e. $Nb/La_N < 1$,

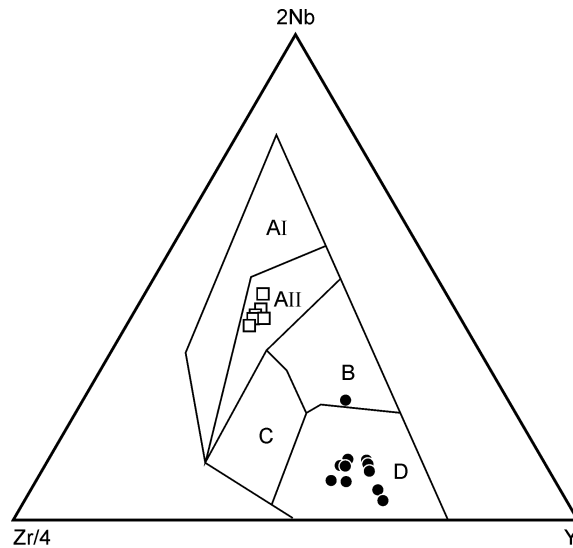


Fig. 9. The Zr/4-2Nb-Y discrimination diagram after Meschede (1986). The fields are defined as follows: AI, within-plate alkali basalts; AII, within-plate alkali basalts and within-plate tholeiites; B, E-type MORB; C, within-plate tholeiites and volcanic-arc-basalts; D, N-type MORB and volcanic-arc basalts. Symbols as in Fig. 7.

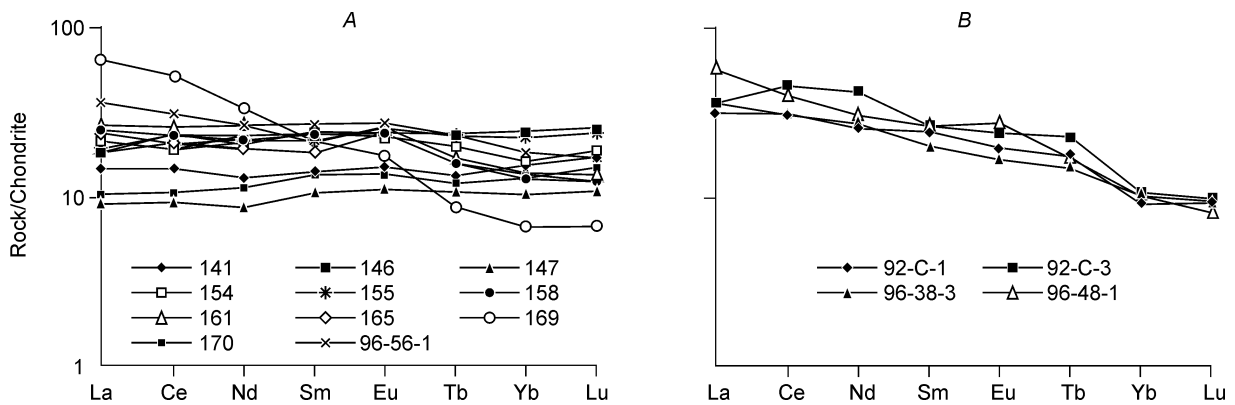


Fig. 10. Chondrite-normalized REE plots for (A) Kurai and (B) Katun' metavolcanic rocks. Normalizing values are from McDonough and Sun [35].

Table 1), unlike continental rift basalts or oceanic island lacking appreciable crustal contamination. Nevertheless, despite the Nb-Ta depletions, we cannot suggest that crustal contamination was a factor in their petrogenesis because of their low Th abundances (Table 1, Fig. 12). The most differentiated basalts (169 and 96-56-1) also show mild Nb-Ta depletion ($(\text{Nb/La})_N = 0.19$ and 0.34 , respectively) and very low Th (0.85 and 0.9 ppm, respectively). These special geochemical features likely have resulted from the contamination of mafic lower crust or lithospheric mantle material [35]. In addition, rather high alkali and LILE contents and moderate Nb depletion may suggest interaction between a mantle plume and a spinel-facies mantle source.

The Kurai samples plot in the MORB field on the Nb/Y versus Nb/Zr diagram, but sample 169 plots closer to the OIB field (Fig. 13, A). In the Nb/Th versus Ti/Yb diagram (Fig. 13, B), the samples form a trend extending from OIB to CLM (continental lithosphere mantle), suggesting mixing or contamination with lithospheric mantle.

Thus, our data indicate that the Kurai metabasalts were possibly formed within oceanic islands, mid-oceanic ridges and/or oceanic plateaus. Their geochemical features (contents of Eu, Cr, Nb-Ta, etc.) are best matched for oceanic plateau basalts formed by fractionation in intermediate chambers.

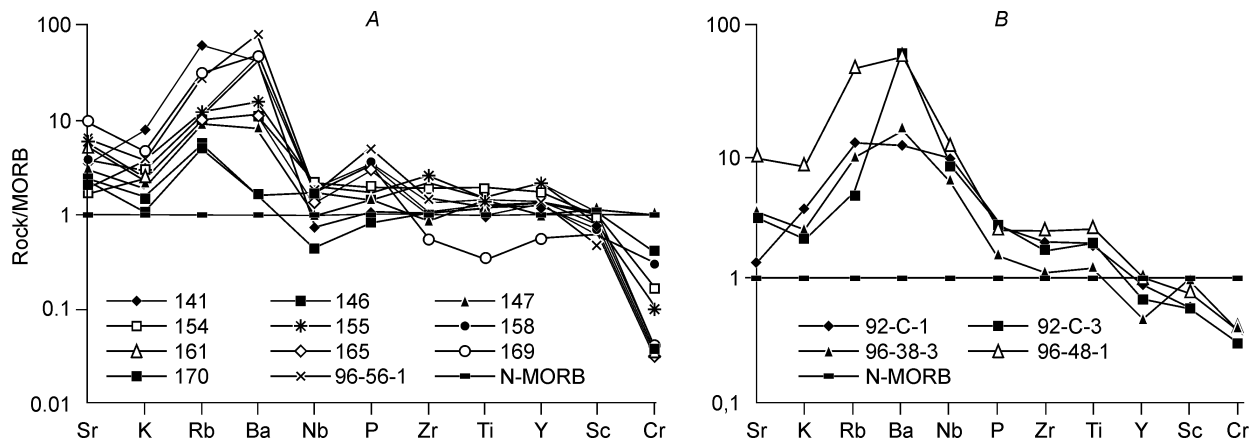


Fig. 11. MORB-normalized REE patterns: A — Kurai, B — Katun'.
The normalizing values are from [35].

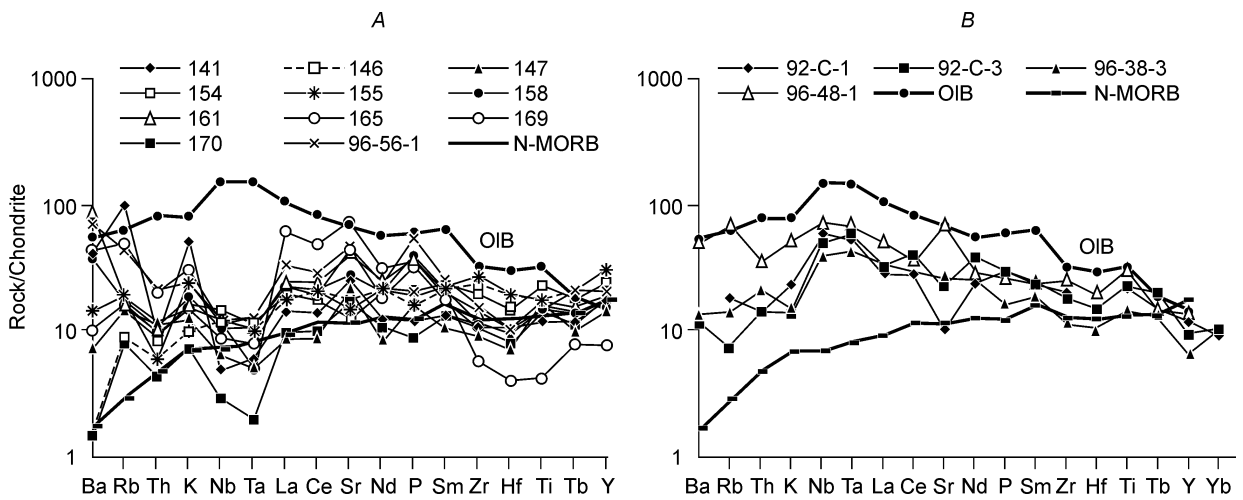


Fig. 12. Chondrite-normalized trace-element diagrams: A — Kurai, B — Katun'. The normalizing values are from [35].

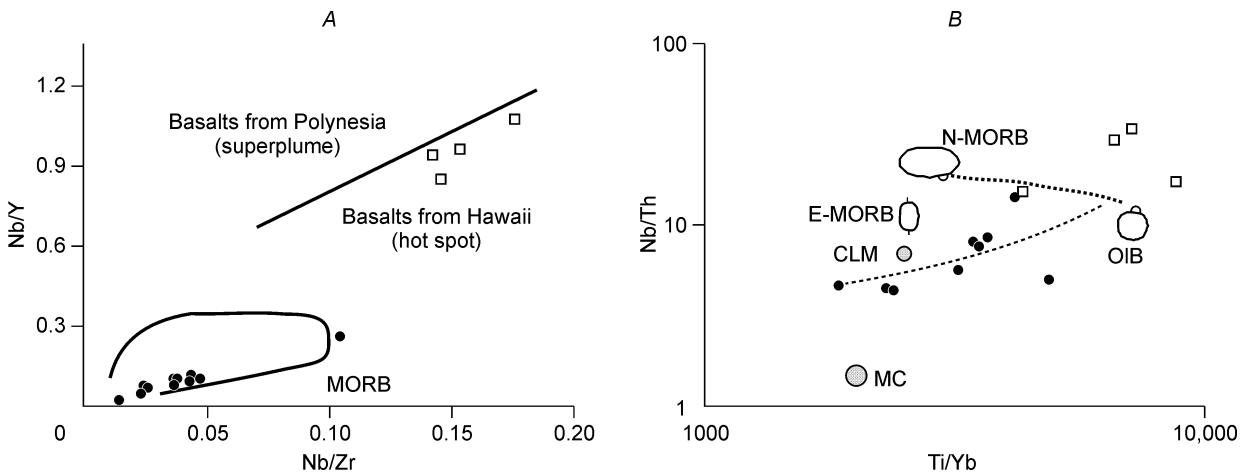


Fig. 13. Nb/Zr vs Nb/Y (A) and Ti/Yb vs Nb/Th (B) plots for Kurai and Katun' volcanic rocks. Data for OIB and MORB are after Sun and McDonough [35], and those for middle crust (MC) and continental lithosphere mantle (CLM) from Li et al. [36]. Symbols as in Fig. 7.

THE STRUCTURE OF THE KATUN' ACCRETIONARY WEDGE

The Katun' accretionary wedge is situated north of the Kurai accretionary wedge and extends over a distance of more than 120 km along the Katun' River, from the Ustyuba River mount (north) to the Edigan River (south) (Fig. 14). It involves three types of rocks composing tectonic sheets. **Type I** consists of dark-gray bitumen-bearing limestones, black siliciliths, dolomites, shales, siliceous shales, and thin basaltic flows. Sedimentary rocks dominate over volcanics. **Type II** includes high-Ti tholeiites and alkaline basalts, their volcanoclastic derivatives, high-carbon siliceous, carbonates and shale sediments. **Type III** consists of bedded reef limestone and dolomite with tuff interbeds. These rock types are suggested to be fragments of a single unit of carbonate, siliceous, terrigenous and ocean island volcanic rocks formed at the oceanic island setting. Type I represents mainly slope facies. Types II and III are the rocks formed at the base of the oceanic island and at its top, respectively. The rocks of the Katun' paleo-island are less altered than the Baratal paleo-island and Katun' carbonate and siliceous sediments have a breccia-like texture and show traces of submarine slumping. Fragments of paleo-oceanic islands occur in association with olistostromes of two types. The first type olistostrome formed during the "collapse" of the Katun' paleo-island and consists only of paleo-island fragments: basalt, chert and limestone. The second type olistostrome consists of the same rocks plus pebbles and boulders of andesite, basaltic andesite, sandstone, mudstone and limestone which could have been transported to the deep trench from an island arc.

There are two types of Vendian-Early Cambrian volcanic rocks in the Katun' paleo-island: (a) thin flows of tholeiitic basalts — relics of oceanic crust — formed in a deep-water setting; and (b) large volcanic buildups and submarine plateaus of alkaline basalts. The first-type volcanic rocks are aphyric tholeiites with sporadic fine phenocrysts of olivine and clinopyroxene which have chemical characteristics of N-MORB. The second type volcanic rocks are olivine-bearing tholeiites, hawaiites, and alkaline basalts. The alkaline basalts contains up to 1–2 cm ultramafic nodules. The microstructure of alkaline volcanics is aphyric or Pl-porphyric (up to 10% plagioclase phenocrysts) with an intergranular matrix containing olivine, plagioclase, and pyroxene. The olivine tholeiites are aphyric. Olivine-plagioclase-pyroxene varieties — hawaiites (MgO = 3–5%) — are porphyric, consisting of olivine (up to 10–15%), pyroxene and plagioclase phenocrysts and glassy matrix.

The Katun' zone has been better studied in terms of paleontology. The rocks of the Katun' paleo-oceanic island contain abundant remnants of microphytoliths, calcareous algae, and sponge spicules indicating their Late Vendian to Early Cambrian age [37]. Detailed description of this sequence and its list of paleontological species were reported by Terleev [37]. This paper provides a brief description of its structure, rock assemblages and microfossils.

The three sites of Edigan, Elandin and Cheposh are the best examples of the structure and rock assemblages of the Katun' paleo-oceanic island. Their location is shown in Fig. 14.

The Edigan site (Fig. 15) is located on the right bank of the Katun', in the water divide of its right tributaries, the Edigan and Cheba Rivers. The Edigan monocline is composed of paleo-oceanic island rocks. There are Late Vendian-Early Cambrian siliceous sedimentary rocks (Eskongo Formation) and oceanic island volcanic rocks of the Manzherok Formation.

The sequence of the Eskongo Formation [37] consists of 16 members (line I—I in Fig. 15):

1. Intercalating thin beds of black limestone, black shales, green-gray tuff-siltstones attaining a total thickness of 60 m.
2. Dark-gray to gray dolomites (up to 15 m) alternating with the above sediments involve lenses of chert and dolomite and attain a thickness of 200 m.
3. Massive and stratified dark-gray/gray dolomites, limestones and tuffaceous shales 60 m thick.
4. Intercalating dark thin-banded limestones and siltstones with chert and dolomite lenses. The thickness is 60 m.
5. Gray to dark-gray, thin-banded and massive dolomites locally contain stromatololiths and microphytoliths (*Osagia* sp., *Nubecularites catagraphus* Reitl.). Subordinate sedimentary rocks are dark limestones, black and greenish-gray tuffaceous siltstones, mudstones, and quartzites. Carbonate rocks laterally change to fine-clastic rocks. Landslides are widespread and contain irregularly shaped bodies of carbonate rocks and siltstones. Total thickness is 450 m.
6. A 400 m thick member compositionally resembles Member 3.
7. Greenish-gray and green massive and schistose volcanics, tuffaceous sandstones and siltstones with subordinate gritstones. The thickness of the member is 180 m.
8. Intercalated shales and dark-gray limestones attain a 140 m thickness.
9. Gray, dark-gray massive and fine-bedded limestones and dolomites frequently contain terrigenous material and abundant microphytoliths (*Osagia* sp.) attaining a thickness of 100 m.

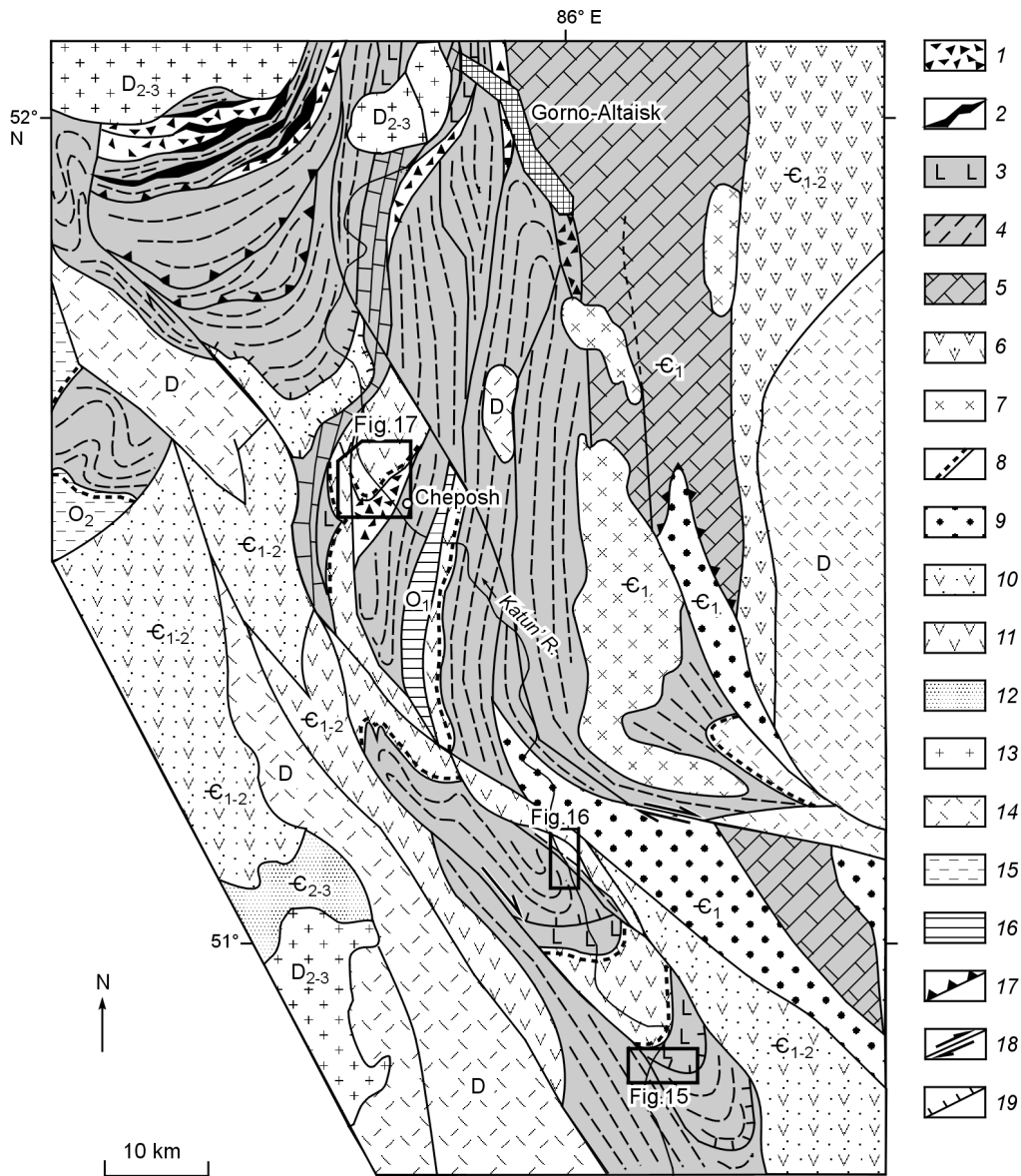


Fig. 14. The geological scheme of the Katun' accretionary wedge with large fragment of the Katun' paleo-oceanic island. 1–5 — Early Cambrian accretionary wedge: 1 — olistostromes and melange, 2 — serpentinite melange, 3 — Vendian-Cambrian paleo-oceanic island basalts, 4 — Vendian-Cambrian slope facies sediments, 5 — Early Cambrian reef limestone and dolomite (carbonate top); 6–8 — Early-Middle Cambrian island arcs: 6 — andesitic basalt and tuff, 7 — gabbroic massifs, 8 — basal conglomerate (Shashkunar Fm.); 9–11 — fore-arc trough: 9 — Early-Middle Cambrian turbidites and andesite-basalt tuffs, 10 — Early-Middle Cambrian turbidite, basalt and tuff, 11 — Early-Middle Cambrian turbidite; 12 — Middle-Late Devonian granitoids; 13 — Devonian volcanogenic-sedimentary rocks; 14 — Middle Ordovician terrigenous-carbonate rocks; 15 — Early Ordovician sediments; 16 — Early Cambrian normal fault; 17 — Late Paleozoic strike-slip fault; 18 — Late Paleozoic thrust.

10. A 400 m thick member is compositionally similar to Member 3 but contains more cherts. Total thickness is 140 m.

11. Gray, dark-gray massive and fine-layered limestones contain separate thin layers of chlorite schists and cherts attaining a 160 m thickness.

12. A 60 m thick member of greenish-gray massive basaltic porphyries.

13. Gray, dark-gray massive and fine-bedded dolomites, locally with clastic material and chert interbeds (1-5 cm thick), and thin limestone and shale interbeds. Total thickness is 120 m.

14. A 300 m thick member compositionally resembles Member 3. Carbonate rocks contain remnants of sponge spicules *Monoxonellida*, *Tetraxonida*, and calcareous algae *Epiphyton* sp.

15. Gray, dark-gray massive and fine-bedded dolomites contain clastic material and microphytoliths *Osagia tenuilamellata* Reitl and attain a thickness of 140 m.

16. Gray and dark-gray limestones and dolomites intercalate with volcanics, tuffaceous shales and quartzites and attain a 200 m thickness.

The total thickness of the section is 3000 m. The Eskongo Formation has a stratigraphic contact with volcanic rocks of the Manzherok Formation. This steeply dipping contact and the presence of overturned beds suggest that siliceous sediments of the Eskongo Formation overlap the Manzherok volcanics. In the section III-IV (Fig. 15) Terleev described calcareous algae *Kordephyton* Rad. et *larites punctatus* Reitl., *N. Catagraphus* Reitl., *Osagia* sp., *Vesicularites flexuosus* Reitl., *Glebosites* sp.; *Korilophyton inopenatus* Voron.; spicules of the sponges *Protospongia* sp., *Chancelloria* sp. There are also dark-gray, gray stromatolite and microphytolite massive and thin-bedded dolomites and limestones with algal bioherms up to 1.5 m high. In the strike, stromatolith dolomites often grade into clastics. The clasts measuring usually tens of centimeters, reaching even few meters, are represented by the same stromatolith and microphytolith dolomites and limestones. They contain the calcareous algae: *Epiphyton* sp., *Korilophyton* sp., microphytoliths: *Osagia tenuilamellata* Reitl., *O. columnata* var. *Ovsianica* Yaksch., *O. aff. Columnata* var. *baicalica* Yaksch., *O. donatella* Korol., *Nubecularites alicarius* Yaksch., *Ambigolamellatus horridus* Z.Zhur., *Volnatella zonalis* Nar., *Confetra* sp., *Vesicularites* sp.

The Elandin site is located in the Katun's right bank, near its right tributary, the Chechkish Brook (Fig. 16). Of special interest are Early Cambrian reef dolomites, which are supposed to form at the top of a paleo-oceanic island. The dolomites overlap volcanic rocks of the Manzherok Formation. An interbed of sedimentary breccia consisting of volcanic boulders and pebbles is found at the base of the dolomite sequence.

The light-gray to gray massive and clastic dolomites contain stromatoliths and microphytoliths and attain a thickness of 250 m. The microphytoliths are *Nubecularites punctatus* Reitl., *N. catagraphus* Reitl., *Osagia* sp., *Vesicularites flexuosus* Reitl., *Ves. lobatus* Teirl., *Ves. bothrydiophormis* (Krasn.), *Ves. reticulatus* Varizh., *Ves.*

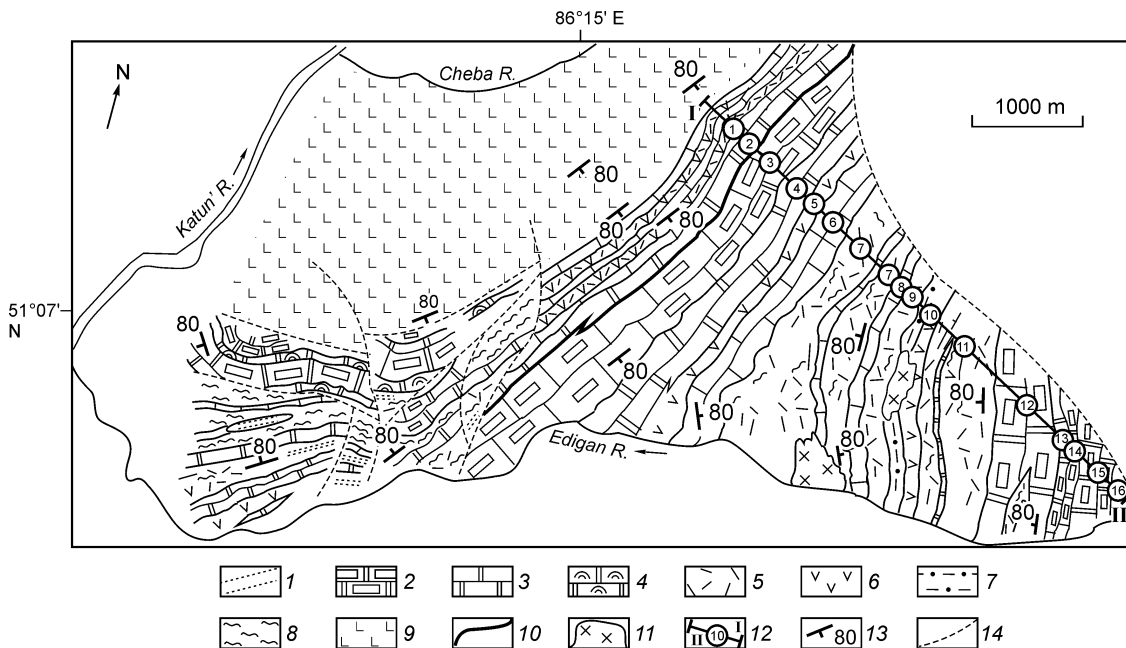


Fig. 15. The geological sketch of the Edigan site of the Katun' paleo-oceanic island (modified after [37]). 1-8 — Eskongo Fm.: 1 — mudstone, 2 — dolomite, 3 — limestone, 4 — stromatolite, 5 — tuff, 6 — porphyry basalt, 7 — sandstone, 8 — chert; 9 — OIB of the Manzherok Fm.; 10 — Precambrian/Cambrian boundary; 11 — gabbro intrusions; 12 — section line and member numbers; 13 — bedding elements; 14 — faults.

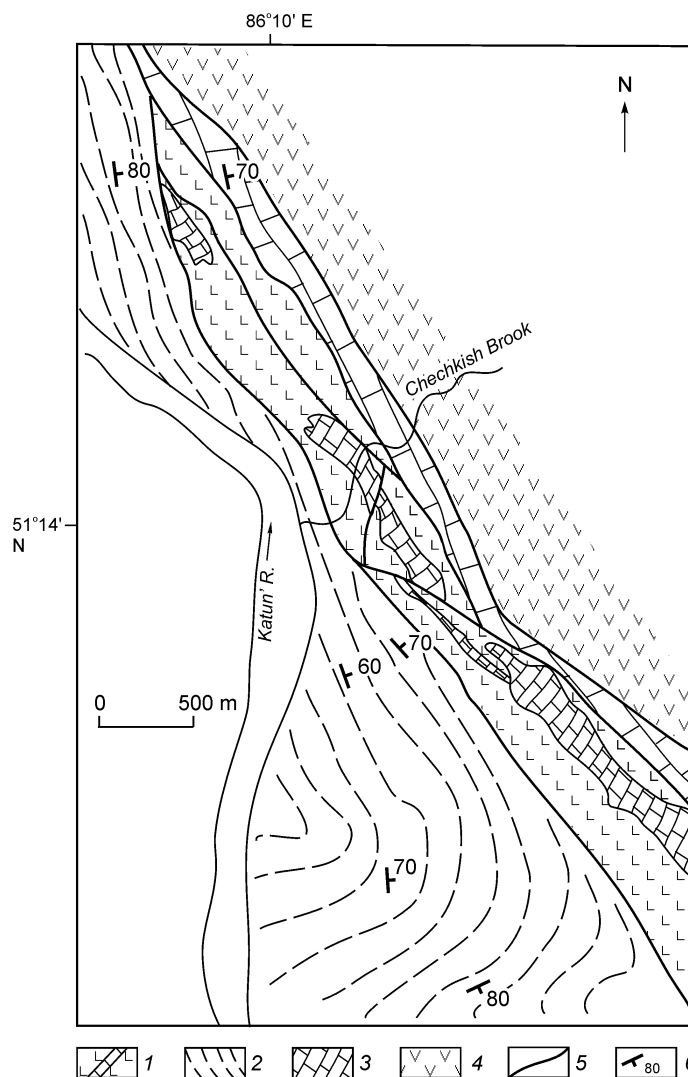


Fig. 16. The geological sketch of the Elandin site of the Katun' paleo-oceanic island (from [37] with modifications). 1 — Manzherok Fm. basalt and lenses of limestone (Vendian), 2 — slope facies basalt, limestone and chert of the Eskongo Fm. (Vendian-Early Cambrian), 3 — Late Vendian-Early Cambrian reef dolomite, 4 — Early-Middle Cambrian basalt and tuff, 5 — fault, 6 — dips and strikes.

igaricus Milstein, *Ves. compositus* Z. Zhur., *Ves. pusillus* Zabr., *Nubecularites uniformis* Z. Zhur., *Ambigolamellatus horridus* Z. Zhur., *Radiosus sphaericus* Z. Zhur., *Volvatella vadosa* Z. Zhur., *Glebosites gentilis* Z. Zhur., *Osagia tenuilamellata* Reitl., *Vesicularites textus* Klinger.

The microphytoliths *Nubecularites punctatus* and *N. catagraphus* and alga *Girvanella sp.* indicate a Late Vendian-Early Cambrian age for the dolomites [37].

The Cheposh site (Fig. 17) is located in the Katun' valley, between Ust'-Syoma and Cheposh Villages (Fig. 14). There, the tectonic sheets composed of paleo-oceanic island rocks alternate with two types of deformed olistostrome. The accretionary wedge is overlapped by basal conglomerates and then Early Cambrian (Sanashtyol Horizon) — Middle Cambrian sedimentary-volcanogenic rocks of a normal island arc [13].

The sequence in the right bank of the Katun' River (line I—II in Fig. 17) includes several tectonic thrust sheets consisting of paleo-oceanic island rocks and melanged olistostromes:

1. A tectonic thrust sheet composed of Type I and Type II olistostromes. The Type I siliceous-carbonate-basaltic olistostrome consists of olistoliths incorporated into the breccia-sandstone matrix. Figure 18a shows the

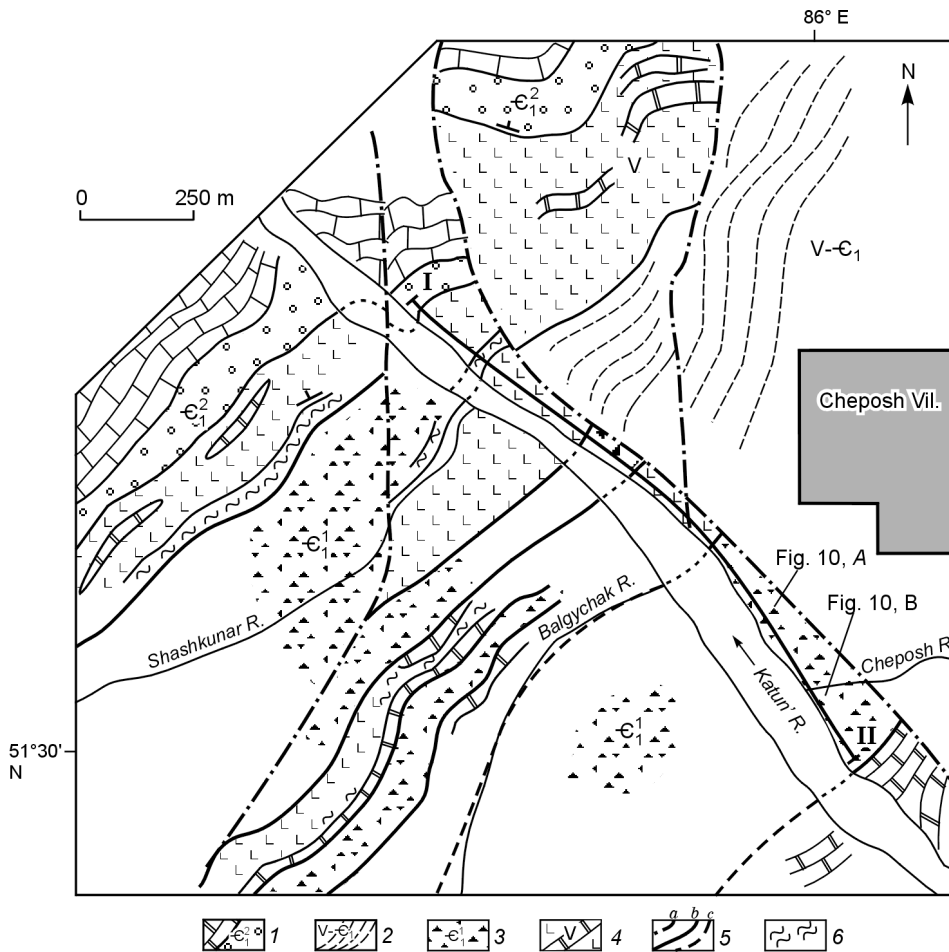


Fig. 17. The geological sketch of the Cheposh site of the Katun' paleo-oceanic island (from [37] with modifications). 1 — Early Cambrian limestone and conglomerate of the Shashkunar Fm., 2 — Vendian-Early Cambrian slope facies basalt, limestone and chert of the Eskongo Fm., 3 — Early Cambrian olistostromes and melange, 4 — Manzherok Fm. basalt and lenses of limestone (Vendian), 5 — fault (*a* — Late Paleozoic, *b* — Early Cambrian, *c* — supposed), 6 — chert.

structure of a fine-clastic olistostrome where olistoliths are several tens of centimeters in length. Large olistoliths are several hundred meters long and tens meters thick and consist of basalts and carbonate rocks.

The Type II olistostrome consists of olistoliths and fine-clastic siliceous-carbonate-basaltic rocks and well-rounded boulders and pebbles of basaltic andesite, andesite, tuffs, sandstones, siltstones, and gray stratified limestones. Figure 18, *B* shows an outcrop in the left bank of the Cheposh mouth and the arrangement of boulders and pebbles in the sand-siltstone matrix composed of clasts of volcanic rocks, cherts, and carbonate rocks. The boulders attain 20 cm in length. The total thickness of the sheet exceeds 300 m. Both olistostromes have been schistosed and display a typical lineation.

2. Intense deformation zone composed of greenschists with blocks of basalt, chert and dolomite attains a thickness of 2–3 m.

3. A 120 m thick siliceous-carbonate-basaltic tectonic sheet.

4. Deformation zone similar to 2.

5. The 8–10 m thick Type I olistostrome.

6. Deformation zone similar to 2.

7. A 150 m thick tectonic sheet composed of pillow lava.

8. Greenschists after 1–2 m thick basalts.

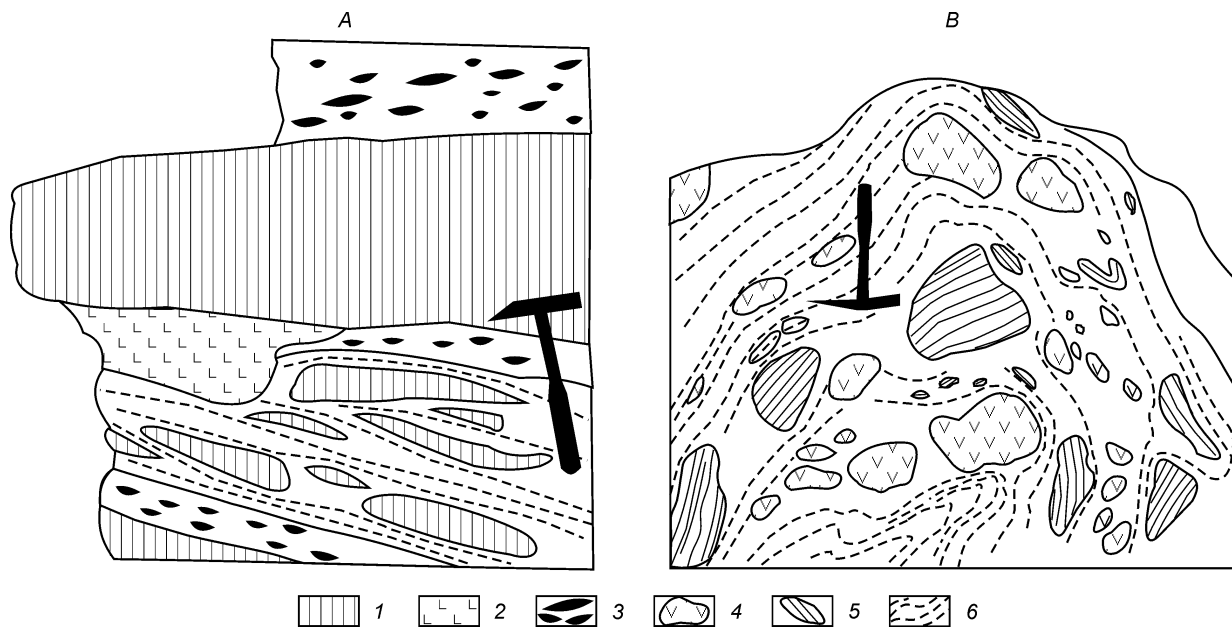


Fig. 18. Two types of tectonized olistostrome-conglomerate from the Katun' River bank, near Cheposh Village (see Figs. 14, 17): A — olistostrome, B — polymictic conglomerate. 1 — chert, 2 — oceanic basalt, 3 — breccia with fragments of oceanic basalt, 4 — andesite and basaltic andesite boulders and pebbles, 5 — pebbles and boulders of chert, sandstone, siltstone and tuff, 6 — bedding in the sand-clay matrix.

9. A 6 m thick tectonic sheet of black cherts.

10. Basaltic and carbonate rocks that outcrop after a 80 m break are 6 m thick.

The Katun' accretionary wedge is overlain by basal conglomerates containing carbonate rocks of the Shashkunar Formation, which occur in the lowest position of the Early-Middle Cambrian island arc sequence. The Early-Middle Cambrian age (Botomian-Amgian) of the island arc comprising the carbonate-terrigenous rocks of the Cheposh and Barangol Formations and volcanic rocks of the Ust'-Syoma Formation is evidenced by numerous archaeocyathan and trilobites (Repina and Romanenko, 1978). The tectonic sheets of the accretionary wedge and carbonate rocks of the Shashkunar Formation are cross-cut by island-arc dikes of pyroxene-plagioclase porphyries, diabase, and gabbro. The dikes preserve the original orientation and are only locally deformed. They are comagmatic with the volcanic rocks of the Ust'-Syoma Formation in the Katun' zone (Fig. 14).

The Early-Middle Cambrian rocks of the normal island arc do not exhibit greenschist facies metamorphism in contrast to the accretionary wedge rocks suggesting a large tectonic re-building which took place in Early Cambrian time (pre-Shashkunar phase).

Thus, the presence of calcareous algae and sponge spicules suggests that the Katun' paleo-oceanic island is of Late Vendian-Early Cambrian age [37]. The Katun' rocks are discordantly overlain by late Early-Middle Cambrian island-arc units.

It is interesting that the reef limestones and dolomites with tuff interbeds, which are supposed to form at the top of a paleo-oceanic island, contain numerous Early Cambrian microphytoliths and calcareous algae. Microphytoliths, sponge spicules and calcareous algae occur in the brecciated dolomites of the Katun' paleo-oceanic island slope facies rocks (Eskongo Formation).

The volcanogenic-sedimentary rocks of the Early-Middle Cambrian normal island arc stratigraphically overlie, through the basal conglomerates, different structural elements of the accretionary prism, which can be seen in many sites of the Katun' zone (Fig. 14). The volcanogenic-sedimentary rocks are characterized by calc-alkaline volcanic rocks and contain Early-Middle Cambrian archaeocytes, brachiopods, and radiolarians (Sanashtogol Horizon) [13].

Volcanogenic, siliceous-limestone and carbonate paleo-oceanic units extend to the northeast, from the Katun' terrane to Gornaya Shoria, and form a 40×250 km structure. In the northwestern part of the Katun' accretionary wedge, the tectonic sheets and olistostromes are surrounded by serpentinitic melange and basalts with N-MORB

characteristics [13]. The melange consists of chrysotile-antigorite schists containing blocks of ultramafic rocks, pyroxenite and gabbro.

COMPOSITION OF BASALTS OF THE KATUN' ACCRETIONARY WEDGE

Whole-rock analyses of metabasaltic rocks from the Katun' accretionary wedge are given in Table 1. The Katun' basalts belong to the low-temperature greenschist facies of regional metamorphism. The pillows consist of Cpx-porphyrific basalt cemented by inter-pillow siliceous-carbonate sediments. Clinopyroxene is partly or completely replaced by chlorite and epidote and the matrix comprises actinolite, epidote, chlorite, and albite. The Katun' metabasalt rocks are mainly classified as alkaline basalts according to alkali-silica ratio (Fig. 7, A), where the compositional points fall in the fields of basalt, trachybasalt and basanite. In the Nb/Y versus SiO₂ diagram three samples are alkaline basalts and one sample is nephelinite basanite. These rocks display a clear Fe-enrichment trend with advancing fractionation and TiO₂ increase with FeO*/MgO (Fig. 8, A, B). These trends are close to those characteristic of strongly differentiated tholeiitic suite [38]. In general, the Katun' samples have similar TiO₂ contents and FeO*/MgO ratios ranging mostly from 1.25 to 2.1, which show a medium degree of differentiation (Fig. 8, B). As far as Na, K, and low-field-strength elements are mostly mobile and susceptible to change during alteration [39], only immobile HFSE and REE were used to identify the magmatic affinity and petrogenesis of these altered mafic volcanic rocks.

Contents of TiO₂ and P₂O₅ range from 1.52 to 3.07 wt.% and from 0.17 to 0.31 wt.%, respectively. Content of Al₂O₃ ranges from 12.4 wt.% to 14.8 wt.%, which is on average a little lower than in IAT. Similar to the Kurai metabasalts, the Katun' mafic volcanic rocks are slightly depleted in LILE (possibly due to the alteration) and enriched in HFSE, Cr and Mg compared to IAT (Table 1; [31]). The samples have high K/Rb and K/Ba ratios, Zr/Nb ratios below 20, intermediate Nb/Zr (0.14–0.18) and Nb/Y bulk ratios (0.86–1.08) (Fig. 13, A). In the 2Nb-Zr/4-Y diagram the samples plot in the field of plume-type basalts, i.e. Hawaiian-type within-plate alkali basalts (Fig. 9).

REE patterns show obvious LREE enrichment (Fig. 10) with La_N = 30–54, (La/Yb)_N = 3.3–5.4. A small Eu maximum is present only on the curve of sample 96-48-1. MORB-normalized trace element patterns show that Y, Sc and Cr are more depleted than MORB but other HFSE are enriched (Fig. 11). No Nb-Ta and Ti depletions have been found. In chondrite-normalized spidergrams (Fig. 12) the Katun' metabasalts display mild Nb-Ta enrichments relative to La (i.e. Nb/La_N > 1). In the Nb/Y versus Nb/Zr and Ti/Yb versus Nb/Th diagrams the samples plot in the field of Hawaiian OIB (Fig. 13, A, B; [35]). Thus, the obtained geochemical data indicate that the Katun' metabasalts are similar to many alkaline basalts of oceanic islands formed without crustal contamination (Table 1; [31, 40]). The Katun' metabasalt represent a within-plate volcanic series, which possibly formed within an oceanic island environment related to hot spots or mantle plume at a low degree of melting of a mantle source. No MORB-type basalts are discussed here.

DISCUSSION AND CONCLUSIONS

Thus, Gorny Altai is a well-preserved geological entity, which recorded the Vendian-Cambrian history of accretionary wedge formation. The processes of the Paleo-Asian oceanic crust formation and collision of large paleo-oceanic island with an island arc within the subduction zone can be reconstructed there.

The Vendian-Early Cambrian subduction of the Paleo-Asian ocean beneath the Siberian continent gave rise to the Uimen'-Lebed' island arc of Vendian age. Hot spots were active within the ocean to form oceanic islands and seamounts.

Study of paleovolcanic constructions within the Pacific folded frame around Eurasia and their present-day analogues [5–8, 12, 45] shows that there were two types of hot-spot-related structures: paleo-oceanic islands and submarine oceanic plateaus. Within old folded areas, fragments of paleo-oceanic island and submarine oceanic plateaus are incorporated in tectonic sheets of accretion-collisional zones. This hinders identification of geodynamic origins of basaltic, sedimentary-basaltic and sedimentary terranes. In addition, many accretion-collisional zones comprise terranes formed in different geodynamic environments, e.g. island-arc or Gondwana-derived terranes (for example, carbonate rocks of an exotic terrane of the Kurai accretionary wedge). Due to the complicated structure of the Katun' accretionary wedge, island-arc, mid-oceanic ridge and hot-spot-related magmatic units of different ages were formerly regarded a single series and interpreted as those formed in back-arc setting and comprised sedimentary rocks of isolated depressions of volcanic rises [46].

A typical feature of oceanic islands is thick slope-facies sedimentary sequences. The above described Katun' and Baratal paleo-oceanic islands are characterized by more than 3 km thick sedimentary slope facies (for example,

the Eskongo Formation at the Edigan site) allowing us to estimate the height of the paleo-oceanic island as exceeding 4 km. The formation of oceanic islands proceeds in two stages: (1) active stage — formation of volcanic build-ups and (2) passive stage — subsidence of volcanic island and formation of an atoll with typical carbonate top reef facies. These stages are well recognized in the rock units of the Katun' and Baratal paleo-oceanic islands.

In general, the composition of rocks of Katun' and Baratal paleo-oceanic islands reflects the evolution of oceanic sedimentation. The oceanic rocks are oceanic island shallow-water reef units with a basaltic base, slope carbonate-siliceous facies, deep-water siliceous sediments and breccias of the bottom of submarine slopes.

Geochemical studies of basaltic rocks show that basalts derived from both lower and upper mantle sources may illustrate the history of hot-spot volcanism. According to REE distribution there are two types of rocks: LREE-enriched (OIB) and close to MORB. The REE contents can be influenced by the degree of differentiation, the degree of partial melting and the source concentrations in the mantle reservoir. Evidence for this comes from high variations of LREE abundances relative to chondrite (25–65 for Kurai and 35–55 for Katun' samples), whereas HREE abundances have much smaller ranges, from 6 to 13 times that of chondrite for Kurai and Katun'. The rocks possessing geochemical features of OIB are similar to alkaline and tholeiitic basalts of world-known oceanic island and oceanic plateau basalts [31, 41]. The fragments of oceanic crust have been identified in many folded accretionary belts, for example, in the Cretaceous Idonappu belt of the Urukawa region in central Hokkaido (Japan), whose greenstone rocks are close to volcanic rocks of Gorny Altai accretionary belts as inferred from Nb/Y and SiO₂, FeO, MgO and TiO₂ proportions, and from TiO₂, Al₂O₃ and P₂O₅ abundances [32].

Our data suggest that the oceanic crust of the Paleo-Asian ocean was formed with participation of mid-ocean ridge and hot-spot volcanism, from Vendian to Early Carboniferous. The intra-plate oceanic volcanism resulted in the formation of seamounts and oceanic islands consisting of basalts, limestones and siliceous-terrigenous rocks.

In Gorny Altai, fragments of oceanic crust have been preserved in accretionary prisms and consist of basalts and sediments of paleo-oceanic islands and, to a lesser degree, mid-ocean ridge basalts. The ophiolites have been almost completely “swallowed” by the subduction zone. Thus, study of oceanic islands incorporated in foldbelts is very important and further detailed geochemical, geochronological, lithological, paleomagnetic and paleontological investigation would allow more complete reconstruction of the ancient oceans and a better understanding of the petrologic processes which resulted in the formation of the oceanic lithosphere.

The research was sponsored in parts by grants 02-05-64627 and 03-05-64668 from Russian Foundation for Basic Research and grant 1247.2003.01 from Scientific School Foundation.

REFERENCES

1. Coleman, R.G., *Ophiolites*, 262 pp., Springer Verlag, Berlin, 1977.
2. Dobretsov, N.L., Yu.E. Moldovantsev, and A.P. Kazak, 1977. *Petrology and metamorphism of ancient ophiolites* [in Russian], 201 pp., Nauka, Novosibirsk, 1977.
3. Dobretsov, N.L., and L.P. Zonenshain, (eds.), *Riphean-Paleozoic ophiolites of North Eurasia* [in Russian], 201 pp., Nauka, Novosibirsk, 1985.
4. Nicolas, A., *Structure of ophiolites and dynamics of oceanic lithosphere*, 367 pp., Kluwer Acad. Publ., The Netherlands, 1989.
5. Cloos, M., Lithospheric buoyancy and collisional orogenesis: subduction of oceanic plateaus, continental margins, island arcs, spreading ridges and islands, *Geological Society of America Bulletin*, 105(6), 715–737, 1993.
6. Chekhovich, V.D., On the accretion of oceanic rises, *Geotektonika*, 4, 69–79, 1997.
7. Masson, D.G., L.M. Parson, and J. Milson, Subduction of island at the Java trench: A view with long-range sidescan sonar, *Tectonophysics*, 185, 51–65, 1990.
8. Collot, J.-Y., and M.A. Fisher, The collision zone between the d'Entrecasteaux Ridge and New Hebrides island arc, *Journal Geophysical Research*, 96, 4457–4478, 1995.
9. Von Huene, R., and D.W. Scholl, Observation at convergent margins concerning sediment subduction, subduction erosion and the growth of continental crust, *Reviews of Geophysics*, 29, 279–316, 1991.
10. Dobretsov, N.L., and A.G. Kirdyashkin, Subduction zone dynamics: models of accretionary wedge, *Ofioliti*, 18(1), 61–81, 1991.
11. Dobretsov, N.L., Collision processes in Paleozoic folded areas of Asia and exhumation mechanisms, *Petrologiya*, 8, 451, 2000.
12. Kanmera, K., and H. Sano, Collisional collapse and accretion of Late Paleozoic Akiyoshi island, *Episodes*, 14, 217–223, 1991.
13. Buslov, M.M., N.A. Berzin, N.L. Dobretsov, and V.A. Simonov, *Geology and Tectonics of Gorny Altai*.

Guide-book of excursion, IGCP Project 283, United Institute of Geology, Geophysics and Mineralogy Publ., Novosibirsk, 1993.

14. Buslov, M.M., and T. Watanabe, Intra-subduction collision and its role in the evolution of an accretionary wedge: the Kurai zone of Gorny Altai, Central Asia, *Geologiya i Geofizika (Russian Geology and Geophysics)*, **36**, 1, 82–93(83–94), 1996.

15. Buslov, M.M., I.Yu. Saphonova, T. Watanabe, O. Obut, Y. Fujiwara, K. Iwata, N.N. Semakov, Y. Sugai, L.V. Smirnova, A.Yu. Kazansky, Evolution of the Paleo-Asian ocean (Altai-Sayan region, Central Asia) and collision of possible Gondwana-derived terranes with the southern marginal part of the Siberian continent, *Geosciences Journal*, **5**, 2001, 203–224, 2001.

16. Buslov M.M., T. Watanabe, I.Yu. Saphonova, K. Iwata, and A.V. Travin, A Vendian-Cambrian island arc system of the Siberian continent in Gorny Altai (Russia, Central Asia), *Gondwana Research*, **5**, 781–800, 2002.

17. Berzin, N.A., and N.L. Dobretsov, Geodynamic evolution of southern Siberia in Late Precambrian — Early Paleozoic time, in: Coleman, R.G. (ed.), *Reconstruction of the Paleo-Asian ocean*, 53–70, VSP International Science Publ., Utrecht, The Netherlands, 1994.

18. Dobretsov, N.L., N.A. Berzin, and M.M. Buslov, Opening and tectonic evolution of the Paleo-Asian Ocean, *International Geology Review*, **35**, 335–360, 1995.

19. Zonenshain, L.P., M.I. Kuzmin, and L.M. Natapov, *Geology of the USSR: A plate tectonic synthesis. Geodynamic Monograph Series*, American Geophysical Union, Washington, 1990.

20. Berzin, N.A., R.G. Coleman, N.L. Dobretsov, L.P. Zonenshain, Xiao Xuchang, and E.Z. Chang, Geodynamic map of the western part of the Paleasian Ocean, *Geologiya i Geofizika (Russian Geology and Geophysics)*, **35**, 7–8, 8–28(5–22), 1994.

21. Simonov, V.A., N.L. Dobretsov, and M.M. Buslov, Boninite series in structures of the Paleo-Asian Ocean, *Geologiya i Geofizika (Russian Geology and Geophysics)*, **35**, 7–8, 182–199(157–171), 1994.

22. Watanabe, T., M.M. Buslov, and S. Koitabashi, Comparison of arc-trench systems in the Early Paleozoic Gorny Altai and the Mesozoic-Cenozoic of Japan, in Coleman, R.G. (ed.), *Reconstructions of the Paleo-Asian ocean*, 160–177, VSP International Sciences Publishers, The Netherlands, 1994.

23. Buslov, M.M., T. Watanabe, L.V. Smirnova, Y. Fujiwara, K. Iwata, J. De Grave, N.N. Semakov, A.V. Travin, A.P. Kir'yanova, and D.A. Kokh, Role of strike-slip faulting in Late Paleozoic-Early Mesozoic tectonics and geodynamics of the Altai-Sayan and East Kazakhstan regions, *Geologiya i Geofizika (Russian Geology and Geophysics)*, **44**, 1–2, 49–75(47–71), 2003.

24. Gusev, N.I., Volcanic formations in eastern Gornyi Altai, *Geologiya i Geofizika (Soviet Geology and Geophysics)*, **26**, 5, 28–35(23–29), 1985.

25. Gusev, N.I., Petrochemical peculiarities of Arydzhan Formation of southeastern Gorny Altai, in: *Magmatism and endogenic metallogeny of western Altai-Sayan folded area* [in Russian], 75–77, Novokuznetsk, 1987.

26. Gusev, N.I., Reconstruction of geodynamic regimes for Precambrian and Cambrian volcanism in southeastern Gorny Altai, in: Kuznetsov, P.P., et al. (eds.), *Paleogeodynamics and formation of mineral-rich zones in Southern Siberia* [in Russian], 32–54, OIGGM SO AN SSSR, Novosibirsk, 1991.

27. Zybin, V.A., Stratotype of Baratal Series of Gorny Altai, in: *Geological structure and mineral resources of Altai region* [in Russian], 3–5, Biysk, 1985.

28. Mossakovsky, A.A., S.Y. Ruzhentsev, S.G. Samygin, and T.N. Kheraskova, Central Asian Folded Belt: Geodynamic evolution and forming history, *Geotektonika*, **6**, 3–33, 1993.

29. Dobretsov, N.L., V.A. Simonov, M.M. Buslov, and S.A. Kurenkov, Oceanic and island-arc ophiolites of Gorny Altai, *Geologiya i Geofizika (Russian Geology and Geophysics)*, **33**, 12, 3–14(1–11), 1992.

30. Ota, T., M.M. Buslov, and T. Watanabe, Metamorphic evolution of Late Precambrian eclogites and associated metabasites, Gorny Altai, southern Russia, *International Geology Review*, **44**, 837–858, 2002.

31. Frolova, T.I., and I.A. Burikova, *Magmatic formations in modern geotectonic environments* [in Russian], 319 pp., Moscow Univ. Press, Moscow, 1997.

32. Ueda, H., M. Kawamura, and K. Niida, Accretion and tectonic erosion processes revealed by the mode of occurrence and geochemistry of greenstones in the Cretaceous accretionary complexes of the Idonappu zone, southern central Hokkaido, Japan, *The Island Arc*, **9**, 237–257, 2000.

33. Saunders, A.D., Geochemistry of basalts from the Nauru basin, Deep Sea Drilling Project Legs 61 and 89: Implications for the origin of oceanic flood basalts, in: Moberly, R., Schlanger, S.O., et al. (eds.), *Initial Reports of the Deep Sea Drilling project, U.S. Government Printing Office. Vol. 89*, 499–517, Washington DC, 1986.

34. Pearce, J.A., Trace element characteristics of lavas from destructive plate boundaries, in: Thorpe R.S. (ed.), *Andesites*, 525–548, Wiley, Chichester, 1982.

35. Sun, S., and W.F. McDonough, Chemical and isotopic systematics of oceanic basalts: Implications for mantle composition and processes, in: Sainders, A.D., and M.J. Norry, (eds.), *Magmatism in the Ocean Basins. Geol. Soc. London. Spec. Pub. 42*, 313–345, 1989.
36. Li, X., Zh.-X. Li, H. Zhou, Y. Liu, and P.D. Kinny, U-Pb zircon geochronology, geochemistry and Nd isotopic study of Neoproterozoic bimodal volcanic rocks in the Kandigan Rift of South China: implications for the initial rifting of Rodinia, *Precambrian Research*, **113**, 135–154, 2002.
37. Terleev, A.A., Stratigraphy of Vendian-Cambrian sediments of the Katun' anticline (Gorny Altai), in: Khomentovsky, V.V. (ed.), *Late Precambrian and Early Paleozoic of Siberia* [in Russian], 82–106, UIGGM Publ., Novosibirsk, 1991.
38. Myashiro, A., The Troodos ophiolitic complex was probably formed in an island arc, *Earth Planet. Sci. Lett.*, **19**, 218–224, 1973.
39. Humphris, S.E., and G. Thompson, Hydrothermal alteration of oceanic basalts by seawater, *Geochim. Cosmochim. Acta*, **42**, 107–125, 1978.
40. Garcia, M.O., F.A. Frey, and D.G. Grooms, Petrology of volcanic rocks from Kaula Island, Hawaii: implications for the origin of Hawaiian protoliths, *Contrib. Miner. & Petrol.*, **94**, 461–471, 1986.
41. Frolova, T.I., and I.A. Burikova, Plateau-basalt magmatism and ocean formation, in: *Vexed questions of plate tectonics and possible alternatives* [in Russian], 30–48, IFZ RAN, Moscow, 2002.
42. Nur, A., and A. Ben-Avraham, A., Oceanic plateaus, the fragmentation of continents and mountain building, *Journal of Geophysical Research*, **87**, 3644–3662, 1982.
43. Meschede, M., A method of discriminating between different types of Mid-Oceanic Ridge Basalts and continental tholeiites with the Nb-Zr-Y diagram, *Chemical Geology*, **56**, 207–218, 1986.
44. McDonough, W.F., and S. Sun, The Composition of the Earth, *Chemical Geology*, **120**, 223–253, 1995.
45. Khanchuk, A.I., A.P. Nikitina, I.V. Panchenko, et al., Paleozoic and Mesozoic guyots of Sikhote Alin and Sakhalin, *Dokl. RAN*, **307**, 1, 186–190, 1989.
46. Gibsher, A.S., S.V. Esin, A.E. Izokh, A.D. Kireev, and T.V. Petrova, Cambrian diopside-bearing basalts of the Cheposh zone in Gorny Altai: a model for fractionation of hybrid magmas in intermediate magmatic chambers, *Geologiya i Geofizika (Russian Geology and Geophysics)*, **38**, 11, 1760–1772(1789–1801), 1997.

Editorial responsibility: V.A. Vernikovskiy

Received 11 August 2003